electronics

MDPI

Article

Possibilities of Diffuse Reflectance Spectroscopy in Determining and Operational Control of the Optical Properties of Finely Dispersed Scattering Media

Oleksandra Hotra [1,*], Vladimir Firago [2], Konstantin Shuliko [2] and Piotr Kisała [1]

[1] Department of Electronics and Information Technology, Lublin University of Technology, Nadbystrzycka 38D, 20-618 Lublin, Poland
[2] Department of Radiophysics and Computer Technologies, Belarusian State University, Nezavisimosti Avenue 4, 220030 Minsk, Belarus
* Correspondence: o.hotra@pollub.pl

Abstract: The characteristics of modern portable spectrometers based on photodetector arrays make it possible to create on their basis a new class of devices for operational control of the optical properties of various media. The introduction into the practice of diffuse reflectance spectroscopy with spatial resolution is hampered by the lack of an analysis of the influence of the width of the spectral region used and other sources of measurement uncertainty on the unambiguous determination of the optical properties of finely dispersed scattering materials. This article describes a method of determining the coefficient of local diffuse reflection and calculating the spectral parameters of the reduced scattering and absorption of radiation based on the differences in their shape, which are clearly manifested in a wide range of the spectrum. This allows the reduction in the determination of the desired spectral dependencies to the formation of a residual function that requires varying the values of only two parameters. A method for normalising the recorded spectral dependencies is described, which makes it possible to minimise the influence of the spectral characteristics of the equipment used on the recorded spectral–spatial profiles. Approbation of the method was carried out on examples of processing spectral–spatial diffuse reflection profiles of four samples of finely dispersed scattering structural materials, as well as diffuse reflection profiles of living tissue in the palm thenar region. The sources of uncertainty that affect the uniqueness of the obtained solutions are found, and solutions are proposed to minimise their influence on the desired spectral dependencies. The results obtained indicate the prospects of using the described method for creating equipment for non-destructive control of the optical properties of finely dispersed materials and media, including living tissues and food products.

Keywords: diffuse reflectance spectra; diffusion approximation; optical non-destructive diagnostics; portable spectrometers; scattering and absorption coefficients; spatial resolution spectroscopy (SRS); linear CCD array detector

Citation: Hotra, O.; Firago, V.; Shuliko, K.; Kisała, P. Possibilities of Diffuse Reflectance Spectroscopy in Determining and Operational Control of the Optical Properties of Finely Dispersed Scattering Media. *Electronics* **2023**, *12*, 2893. https://doi.org/10.3390/electronics12132893

Academic Editors: Kan Wu and Junhe Zhou

Received: 9 June 2023
Revised: 23 June 2023
Accepted: 27 June 2023
Published: 30 June 2023

1. Introduction

The problem of non-destructive testing of various materials and media is multifaceted and has several directions for its solution. Optical spectroscopy is widely used in the analysis of media composition [1–3]. A fairly new direction in the optical control of inhomogeneous, strongly scattering media is the spectroscopy of back diffuse reflection of light radiation with spatial resolution [4–7]. The values of the reduced scattering coefficient μ'_s of these media significantly exceed the values of the reduced absorption coefficient μ_a. This leads to the fact that even with a relatively small optical thickness, there is multiple scattering of radiation in the medium. By recording the spectra of radiation reflected back by the medium at different distances between the emitting and receiving fibre-optic probes ρ_k, it is possible to determine its optical characteristics. With their further analysis, it becomes

possible to assess the deviation of the composition of the controlled medium from the predetermined or reference values [4–9]. The potential possibilities of diffuse reflection spectroscopy are attractive for the creation of new small-sized optical-electronic equipment designed for the rapid determination and control of the properties of various scattering media and composite materials. The complexity of the principles of operation of this equipment and the lack of an assessment of the uncertainty of the measurement results, which is due to both the instability of the parameters of the equipment being created and the unknown properties of the media and samples under study, requires a thorough investigation that clarifies the prospects for the considered direction in the development of optoelectronic instrumentation.

The regularities of light scattering in inhomogeneous media are complex [10]. Analytical solutions of the integro-differential equation of radiation transfer in scattering media have not been found [10,11]. Therefore, the search for possible simplifications of this solution in the analysis of the optical properties of strongly scattering media has been carried out for several decades [12–20]. At present, when studying the optical properties of strongly scattering media, the Monte Carlo simulation of photon migration in a medium with given values of the absorption coefficient μ_a, scattering coefficient μ_s, and anisotropy factor g is mainly used [19]. Since this method requires time-consuming numeric calculations, a number of authors have obtained approximate expressions based on the use of the diffusion approximation [21,22] and the photon diffusion scheme with a set of positive and negative radiation sources [14–18,23]. The authors of these approximations compare the obtained dependencies both with experimental ones and with dependencies calculated using the Monte Carlo method and show their applicability when certain limitations are imposed on the values of absorption coefficient μ_a, scattering coefficient μ_s, and anisotropy factor $g = \langle \cos(\Theta_s) \rangle$, where Θ_s is the photon deflection angle during the scattering. The presence of such analytical expressions greatly simplifies the algorithms for fitting (when solving a system of nonlinear equations) the given values of the coefficients $\mu_a(\lambda_0)$ and $\mu'_s(\lambda_0) = \mu_s(\lambda_0)\ (1 - g)$ so that they best correspond to the experimentally obtained dependencies of the local diffuse reflection coefficient $R_m(\lambda_0,\rho_k)$ on the distance between the probes ρ_k, obtained at a wavelength λ_0 [24]. It should be noted here that the complex nonlinear dependency between the experimentally obtained dependencies $R_m(\lambda_0,\rho_k)$ and the values $\mu_a(\lambda_0)$, $\mu_s(\lambda_0)$, and $g(\lambda_0)$, as well as the influence of the state of the surface of the controlled scattering medium, can lead to the ambiguity of the obtained values $\mu_a(\lambda_0)$ and $\mu'_s(\lambda_0)$ when solving the inverse problem since it is not possible to separate their influence on the experimentally obtained dependencies successfully.

The ambiguity in determining the optical properties of finely dispersed scattering media can be significantly reduced by registering the spectral–spatial diffuse reflection profiles in a wide range of the spectrum. Spatially resolved optical spectroscopy provides more information than systems that record the spectra at a fixed distance between the probes. Therefore, the analysis of back diffuse reflection spectra recorded at several distances ρ_k between the illuminating and receiving fibre-optic probes is a promising direction for further development of the discussed methods and equipment. Considering the transformation of the shape of the recorded spectral dependencies that occurs when changing ρ_k, it should, in principle (with the introduction of some assumptions), improve the unambiguity in determining the spectral absorption $\mu_a(\lambda)$ and the reduced scattering $\mu'_s(\lambda)$ coefficients. Absorption of radiation mainly occurs in resonance bands, which are quite wide for condensed media. The scattering of light radiation is determined by the inhomogeneity of the medium and depends on its microphysical parameters. When describing scattering media, elastic scattering of radiation is usually considered, and several types of radiation are distinguished: Rayleigh scattering, Mie scattering, and scattering by optical inhomogeneities. In strongly scattering media, multiple scattering is predominant.

The dimensions of the inhomogeneities of the medium affect the intensity, angular distribution, and spectrum of the scattered radiation. At the average size of inhomogeneities $a < \lambda/15$, Rayleigh scattering dominates, for which the scattered light intensity is propor-

tional to $1/\lambda^4$. With an increase in the size of inhomogeneities or scattering particles, the number of elementary dipoles in them becomes large, and they can be arranged arbitrarily. This requires taking into account the difference in the phases of the re-radiation of electromagnetic oscillations by these elementary dipoles and the distance between them, which leads to the appearance of the corresponding lobes on the scattered radiation pattern. The dependency of the attenuation of radiation on the wavelength becomes much weaker in this case. For example, for water droplets in a cloud with an average radius $a \approx \lambda$, the physical mechanism of Mie scattering is observed, and the scattering cross section is proportional to $\sigma_s \sim a^4/\lambda^2$. This indicates that the scattering coefficient of finely dispersed media usually smoothly decreases with wavelength, and it is often approximated by a power-law hyperbola $\mu_s(\lambda) \sim a_s/\lambda^n$ [5,25], where a_s has the dimension $\mu m^n/cm$ or normalised expression $\mu_s(\lambda) \approx a_0 \cdot (\lambda/\lambda_0)^b$, where a_0 with a dimension of $1/cm$ determines $\mu_s(\lambda_0)$, and b is the slope of the dependency $\mu_s(\lambda)$ [26]. In the presence of a mathematical model that adequately describes the optical characteristics of the medium, the noted differences in the behaviour of the spectral dependencies $\mu_a(\lambda)$ and $\mu'_s(\lambda)$ make it possible to fit the model parameters in a wide range of wavelengths to the experimentally obtained spectral dependencies to provide better solution stability.

Finding a connection between the microphysical and optical characteristics of scattering media is a difficult task. It requires significant effort and time by specialists to calculate radiation patterns and simulate scattering processes [27,28]. Due to the wide variety of such substances, their variability, and the need to verify the created mathematical models, their development, in many cases, will not be commercially viable. Therefore, it is advisable to develop measurement methods that allow the experimental determination of the dependencies $\mu_a(\lambda)$ and $\mu'_s(\lambda)$, which will contribute to the widespread introduction of these methods for monitoring in practice.

Taking into account the potential possibilities of diffuse reflectance spectroscopy with spatial resolution, the aim of the article is the analysis of the possibilities of increasing the unambiguity of determining the spectral coefficients $\mu_a(\lambda)$ and $\mu'_s(\lambda)$ of scattering media using the known diffusion approximations of radiation transfer in a wide part of the spectrum. It is obvious that the unambiguity of determining the spectral coefficients $\mu_a(\lambda)$ and $\mu'_s(\lambda)$ will open up the possibility of a wide application of diffuse reflection spectroscopy with spatial resolution when creating the appropriate small-sized optical-electronic equipment for the operational control of the properties of scattering media and composite materials.

2. Existing Diffusion Approximations

When describing the subsurface radiation transfer in scattering media, it is desirable to simplify the solution of the linearised Boltzmann equation [13,16,28–30] using the angular brightness integrals [11,13]. When considering stationary problems, in the process of simplifying the description, a diffusion approximation is obtained, which makes it possible to describe the radiation brightness at point $\mathbf{r}$ in direction $\vec{s}$ by the expression [11,16]:

$$L\left(\mathbf{r}, \vec{s}\right) = \frac{1}{4\pi}\phi(\mathbf{r}) + \frac{3}{4\pi}J\left(\mathbf{r}, \vec{s}\right) \cdot \vec{s} = \frac{1}{4\pi}\phi(\mathbf{r}) - \frac{3D}{4\pi}[\nabla\phi(\mathbf{r})] \cdot \vec{s}\,, \tag{1}$$

where $J\left(\mathbf{r}, \vec{s}\right) = \int\limits_{4\pi} \vec{s} \cdot L\left(\mathbf{r}, \vec{s}\right) d\Omega$ is the luminous flux from the elementary area in the direction of the unit vector $\vec{s}$, which in the literature is called the current density.

For an infinite homogeneous medium containing a point isotropic source, the solution to Equation (1) is the Green function for diffusion [11,13]:

$$\phi(r) = \frac{\Phi_S}{4\pi D r} e^{-\mu_{\text{eff}} r}\,, \tag{2}$$

where r is the distance from the isotropic source to the surface of a sphere with radius r; Φ_S is the radiation power of an isotropic source, $D = 1/(3\mu'_{tr}) = 1/[3(\mu'_s + \mu_a)]$ is the optical diffusion length, and $\mu_{eff} = \sqrt{\mu_a/D} = \sqrt{3\mu_a(\mu_a + \mu'_s)}$ is the effective coefficient of the attenuation of radiation by the medium. Usually, the units W/cm^2 or W/mm^2 are used for ϕ.

Spatially resolved diffuse reflectance spectroscopy is based on recording the spectra of radiation leaving the surface of a scattering medium at different distances ρ from the input point of the initial photon flux. Therefore, when obtaining analytical expressions describing the local luminosity $M\left(\rho, \vec{s}\right)$ (W/cm^2) or the coefficient of local diffuse reflection $R(\rho)$ (1/cm^2), several simplifying assumptions are used. When a narrow beam of light illuminates a semi-infinite scattering medium with anisotropic scattering, it is replaced by an isotropic radiation source, which is located in the scattering medium at a depth z_0 approximately corresponding to $1/\mu'_s$. This assumption is fulfilled in cases where the absorption coefficient μ_a is small compared to μ'_s. Therefore, the placement depth of an equivalent isotropic source is often chosen equal to one photon's transport mean free path $l_{tr} = 1/\mu_{tr} = 1/(\mu'_s + \mu_a)$ [11].

The authors of [17], using these assumptions, considered the case when the input of radiation into a semi-infinite medium and registration of diffusely reflected radiation is carried out using fibre-optic probes oriented normally to the surface (as shown in Figure 1a), and proposed an approximate analytical expression for calculating the coefficient of directional diffuse reflection of a sample of a semi-infinite medium:

$$R(\rho) = \frac{z_0 S_f}{2\pi}\left[\frac{\mu_{eff}}{\rho^2 + z_0^2} + \frac{1}{\left(\rho^2 + z_0^2\right)^{3/2}}\right] e^{-\mu_{eff}\left(\rho^2 + z_0^2\right)^{1/2}}, \quad (3)$$

where $z_0 = K/\mu'_s$ is the extrapolation length, K is a dimensionless constant, the value of which depends on the anisotropy parameter of the scattering particles and the surface reflection coefficient, and S_f is the area of the end face of the optical fibre probe.

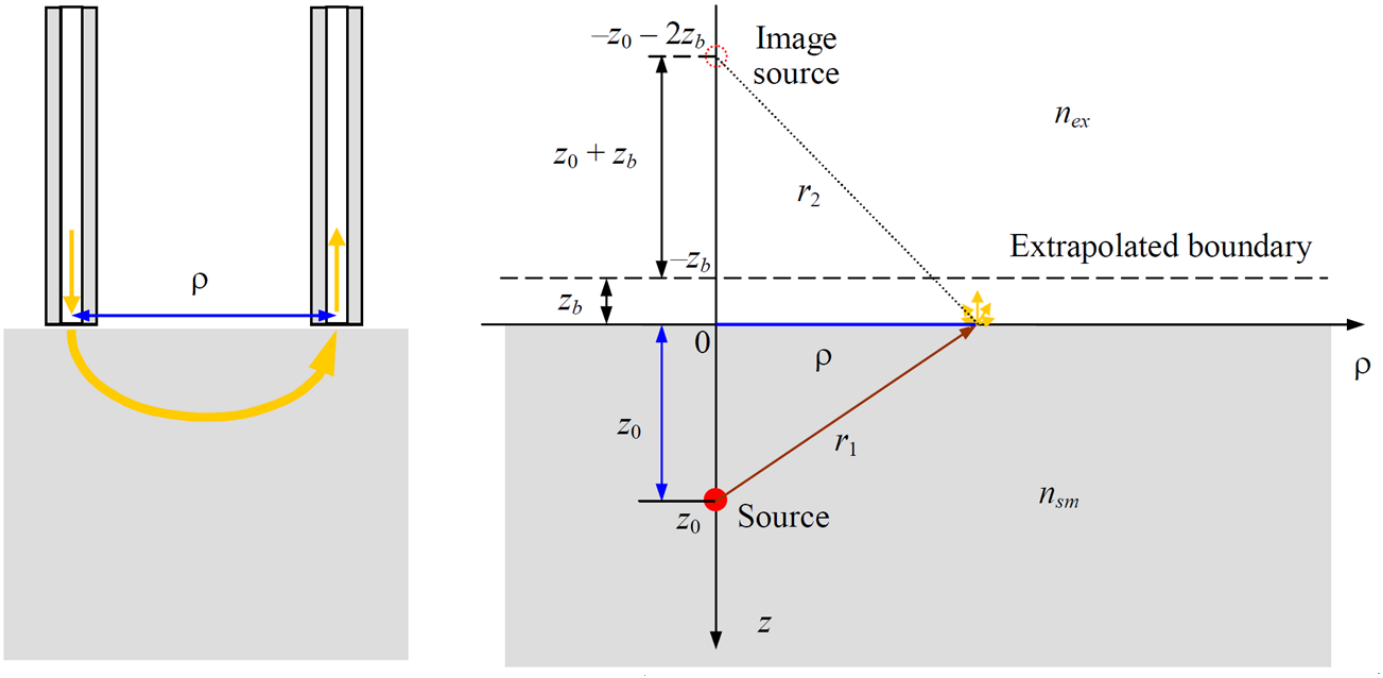

(**a**) (**b**)

Figure 1. Scheme for measuring diffusely reflected light by a scattering medium using fibre-optic probes (**a**) and the geometry of extrapolated model of photon boundary diffusion (used in [14]) (**b**).

The drawback of expression (3) is the need to select the value of K included in z_0, which turns out to be inconvenient in practice. Also, there is no consideration of the refractive indices of radiation of both the scattering medium n_{sm} and the transparent medium n_{ex}, in which the fibre-optic probes are located. The authors of [14,18] proposed a method for solving the diffusion equation, which solves the problem of the adequate setting of boundary conditions and the impossibility of using (2) in a semi-infinite medium. They noticed that when a weakly divergent radiation beam is introduced into a medium with multiple photon scattering, the beam of this radiation can be replaced by an isotropic emitter, which is located under the interface. This allows the introduction of a dipole radiation source shown in Figure 1b, which consists of two point sources located in an infinite homogeneous scattering medium. The first of them is a positive source and is located at a depth of z_0. It is a source of photons and "pushes out" a stream of light from the medium. The second negative source is located higher and simulates the extraction of radiation from the surrounding space [14,15], which hypothetically represents a scattering medium extended upwards to infinity. Therefore, between the sources, there must be an extrapolated boundary on which the values of ϕ are equal to zero, since these two hypothetical sources of different polarity simultaneously affect the light fluxes. It should be located above the interface between the media, i.e., at a distance of z_b, since in the real case, part of the scattered radiation leaves the medium through its surface, i.e., at $z = 0$. It is also assumed that the gradient $\partial\phi(\rho, z)/\partial z$ is in the range $-z_b \leq z \leq 0$ and changes linearly [14,15].

Since it is necessary to take into account the influence of both hypothetical radiation sources on the light fluxes, we obtain that at $z = 0$, the flux density is as follows:

$$\phi(\rho, z = 0) = \frac{\Phi_S}{4\pi D}\left(\frac{1}{r_1}e^{-\mu_{\text{eff}}r_1} - \frac{1}{r_2}e^{-\mu_{\text{eff}}r_2}\right), \tag{4}$$

where $r_1 = \sqrt{z_0^2 + \rho^2}$, $r_2 = \sqrt{(z_0 + 2z_b)^2 + \rho^2}$.

Careful consideration of the boundary conditions [15,30–34] makes it possible to find an expression for the local diffuse reflection coefficient of this semi-infinite medium in the form of two components, which are determined through the illumination ϕ of the scattering medium by the dipole source and the diffusion component j [14,18]:

$$R(\rho) = k_\phi(n_{sm})\frac{\phi(\rho, z = 0)}{\Phi_S} + k_j(n_{sm})\frac{j_z(\rho)}{\Phi_S}, \tag{5}$$

where

$$j(\rho) = -D\left.\frac{\partial\phi(\rho)}{\partial z}\right|_{z=0} = \frac{\Phi_S}{4\pi}\left[\frac{z_0}{r_1^2}\left(\mu_{\text{eff}} + \frac{1}{r_1}\right)e^{-\mu_{\text{eff}}r_1} + \frac{z_0 + 2z_b}{r_2^2}\left(\mu_{\text{eff}} + \frac{1}{r_2}\right)e^{-\mu_{\text{eff}}r_2}\right], \tag{6}$$

$$k_\phi(n_{sm}) = \frac{1}{2}\int_0^{\pi/2}\left[1 - R_{fr}(\Theta, n_{sm})\right]\sin(\Theta)\cos(\Theta)d\Theta, \tag{7}$$

$$k_j(n_{sm}) = \frac{3}{2}\int_0^{\pi/2}\left[1 - R_{fr}(\Theta, n_{sm})\right]\sin(\Theta)\cos^2(\Theta)d\Theta, \tag{8}$$

Θ is the angle of incidence of radiation from the medium relative to the normal to the surface directed into the medium, and $R_{Fr}(\Theta, n_{sm})$ are the Fresnel formulas for unpolarised light [32]. Additionally, when setting the boundary conditions necessary for solving differential Equation (1), we used the ratio $A = (1 + R_{\text{eff}})/(1 - R_{\text{eff}})$, which depends on the effective reflection coefficient R_{eff} of radiation incident from a semi-infinite medium onto the interface between the media, into the back hemisphere, the expression for which was obtained by the authors of [32].

The authors of [18] experimentally confirmed the possibility of using the considered diffusion approximation (5) in calculating $R(\rho)$ of a phantom in the form of a polystyrene plate (matrix) 22 mm thick with a refractive index n_{sm} = 1.59 and a filler in the form of titanium oxide particles TiO_2. The influence of the refractive index n_{ex} was checked by replacing the air medium ($n_{ex} \approx 1$) above the phantom with a layer of water with $n_{ex} \approx 1.333$. In the expression given in [18], the values of k_Φ and k_j were 0.089 and 0.239, respectively (0.239 close to $3/4\pi$) in the air above the phantom and 0.169 and 0.406 in the case of using a thick layer of water above the phantom. Other experimental measurements [15,24] confirm the possibility of determining the optical characteristics of phantoms with a relative root-mean-square error of about 10–20%.

Comparison of the results obtained using the diffusion approximation with the results of the Monte Carlo simulation $R(\rho)$ [15,24] shows that the diffusion approximation with one dipole source poorly describes the dependency of the local reflection coefficient $R(\rho)$ at small values $\mu_{eff.}\rho < 0.7$. A detailed discussion and corresponding graphical dependencies can be found in [15,24]. Interest in the clinical use of the diffusion approximation in single-probe endoscopes with a set of optical fibres has caused the need to overcome the noted drawback of the diffusion approximation, i.e., the incorrect description of the aggressive diffuse reflection peak near the point where the radiation enters the tissue. The authors of [23] proposed a modification of the model with one dipole source, supplementing it with one more auxiliary dipole source. These positive and negative auxiliary sources are located much closer to the surface of the scattering medium than the main ones, which makes it possible to simulate an aggressive peak of diffusely reflected radiation in the vicinity of the point where the radiation enters the tissue due to the pumping of a part of the diffusely reflected light radiation into it by the regions of the medium with large values of ρ. We have used the analytical expressions for calculating $R(\rho)$ in order to assess the possibility of using the three considered diffusion approximation models [14,17,23] when determining the spectral indices $\mu'_s(\lambda)$ and $\mu_a(\lambda)$ of several scattering materials in the spectral range from about 420 to 1130 nm.

3. Experimental Setup

The study of the possibilities of spatially resolved diffuse reflectance spectroscopy was carried out using computerised experimental equipment based on fibre-optic technology and an AvaSpec 2048WL compact spectrometer manufactured by Avantes (Apeldoorn, The Netherlands). The operation of the installation is controlled using a program created by the authors of this article in the C# integrated development environment. The graphical interface of the program has all the necessary elements for control and a window for displaying the resulting family of spectra View in the form of 10 graphic diffuse reflection spectra obtained at different distances ρ between the emitting and receiving probes. It provides calibration of the initial position of the movable probe, selection of measurement settings, acquisition of families of spectra, as well as visualisation and storage of the recorded series of measurements of families of diffuse reflection spectra.

Light radiation was introduced into the scattering medium, and the diffusely reflected flux was recorded using two identical FC-UVIR600-1-1.5 × 100 fibre-optic probes with needle-shaped tips. The length of these tips, equipped with a steel shell, is 100 mm, and the diameter is 1.5 mm. To ensure a good signal-to-noise ratio in these probes, a quartz fibre with a light guide diameter of 600 μm, numerical aperture NA = 0.22, and a normalised operating spectral range from 200 to 2500 nm was used. The opposite ends of the fibres used are equipped with SMA connectors for connecting probes to radiation sources and the spectrometer.

The probes were fixed in a special device, which ensures both the holding of the probes in a vertical position and the possibility of precise movement of the end of one needle-shaped tip relative to the end of the second fixed one using a stepping micromotor. This motor is controlled by the A4988 stepper motor driver, which receives control signals generated by the Arduino nano microprocessor. The Arduino microprocessor is connected

to the control PC via the USB interface. Figure 2 shows the layout of the ends of fibre-optic tips and their positions used in experimental measurements. The minimum possible distance between the fixed and movable ends of the probes h is 2.2 mm, since a blackened duralumin partition d_p = 0.7 mm thick is installed between them. The length of the limiting slot, in which the end of the movable probe moves, is chosen to be 17.2 mm. This provides a symmetrical displacement of the end of the movable probe to the left and to the right from the central position by about 7.85 mm. Such a scheme of the symmetrical position of locations x_k of the movable probe was chosen to control the effect of surface roughness on the obtained diffuse reflection spectra since, for a smooth surface, these spectra obtained to the right and left of the emitting probe should coincide. The distance between the surface of the sample under study and the ends of the fibre-optic probes was chosen to be 0.1–0.2 mm so that there was no direct contact of the ends with the sample.

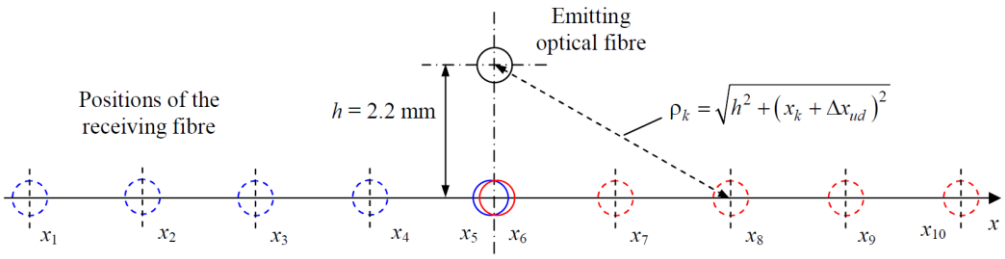

Figure 2. Scheme of the used positions of the light guide end of the movable receiving probe relative to the centre of the light guide end of the fixed emitting optical fibre.

To illuminate the studied samples of scattering media, two radiation sources were used: an AvaLight-HAL-S-Mini halogen radiation source and a source using an ultra-bright white light emitting diode (LED) TDS-P005L8011. They have SMA connectors for connecting a fibre-optic probe. The AvaLight-HAL-S-Mini uses a 10W halogen lamp and focusing optics to provide the minimum required flux at the fibre probe output from 350 nm to 2500 nm. The halogen source is equipped with a controlled TTL shutter, which blocks the flux from the lamp during the registration of the background radiation spectrum. This background spectrum is subtracted from the obtained spectra in order to eliminate the influence of the dark current of the spectrometer linear CCD array and external background light sources.

The LED radiation source is used to study dense, highly scattering media in the visible region of the spectrum from 410 to 750 nm.

To reduce the uncertainty Δx_{ud} of setting the position of the centre of the end face of the movable probe relative to the centre of the end face of the fixed x_k, the initial reference position of the end face of the movable probe must be calibrated before measurements. To carry this out, the end face of the movable probe is moved by a stepper motor, first to the left until it stops against the wall of the guide slot, and then to the right closer to the centre, and the spectrometer registers step by step in each of the positions the total spectral fluxes $I_\Sigma(x)$ formed by diffuse backscattering of the test sample, which are collected by a movable probe. Further, the maximum of this dependence is found, which corresponds to the zero position of the centre of the end of the movable probe. To eliminate the influence of external illumination, the shutter of the halogen lamp is periodically closed at each step of the movement, and the background flux is measured. It is subtracted from the flux recorded with the shutter open. The x value corresponding to the maximum of the dependence $I_\Sigma(x)$ is taken as the initial reference position. The control program provides the ability to select up to 10 positions of the movable probe relative to the fixed ones. If the signal-to-noise ratio of the recorded spectra is insufficient, it is possible to carry out their digital accumulation with subsequent averaging over N_k realisations. There is also the possibility of preliminary automatic determination of the required exposure time τ_k so that the maximum values of the recorded spectra would be near the values of 40,000 readings of the ADC of the spectrometer. The selected settings can be saved to a file on the hard disk and used when conducting a repeated series of measurements.

4. Method of Measurement and Processing of Spectral Dependencies

When carrying out experimental measurements of the spatial–spectral profile of the diffuse reflection coefficient $R(\lambda,\rho_k)$, a number of difficulties arise, without overcoming which it is impossible to adequately use the diffusion approximation. A significant problem is the need to exclude the influence of the spectral characteristics of the equipment used, including the spectral characteristics of the source of light radiation introduced into the scattering medium. Also, when taking into account the influence of the refractive index of the matrix of the scattering medium n_{sm} on the values of coefficients k_Φ and k_j, it is necessary to justify the choice of the internal reflection coefficient R_{eff}. Here, it is necessary to take into account the state of the surface of the sample under study, since the Fresnel equations are applicable only for homogeneous materials with a smooth surface. Another difficulty is the need to strictly keep the parameters of the measurement scheme and ensure the optimal choice of the positions of the movable probe ρ_k used in obtaining a family of local diffuse reflection spectra.

The spectral characteristics of the equipment used in spatially resolved diffuse reflectance spectroscopy are usually taken into account by normalising the recorded spectral dependencies to the spectral dependency $V_{Wnorm}(\lambda,\rho_0)$ obtained for a white diffuse reflectance standard normalised to unity. Pressed polytetrafluoroethylene (PTFE) powder is used as a material for such white reference reflectors [35]. The spectral reflection coefficient of such standards is measured using an integrating sphere at the normal incidence of the initial radiation beam. Diffuse reflectance standards made of this material in the spectral range of 300–1700 nm have a radiation reflection coefficient of about 98–99%. They are widely used in spectroscopy and are usually supplied with spectrometers, for example, the diffuse reflectance standard WS-2 from Avantes. Despite the good reflective properties of this material, it cannot be considered an isotropic scattering medium, since it is sintered from powder and does not have a homogeneous base, the so-called matrix. The light radiation falling on its surface, due to the presence of numerous air microcavities, is quickly re-radiated back already in a thin (about 2 mm) surface layer. Therefore, approximately 98% of the incident flux is reflected back by the reference white reflector WS-2.

Manufacturers of compact spectrometers based on photodetector arrays usually do not calibrate them according to the intensity of the recorded radiation fluxes. Therefore, the obtained initial spectra as the dependencies of digital counts $D_s(\lambda_i)$ on wavelengths λ_i, where the index i denotes the i-th element of the array, are distorted by the spectral characteristics of the equipment used. It is also necessary to take into account the integration time τ_k of the photocurrents generated by the photosensitive elements of the photodetector arrays, i.e., in further calculations, the ratio $V(\lambda,\rho_k) = D_s(\lambda_i,\rho_k)/\tau_k$ should be used. After normalising the obtained dependencies to the calculated dependency $V_{Wnorm}(\lambda,\rho_0) = [V(\lambda,\rho_5) + V(\lambda,\rho_6)]/\max[V(\lambda,\rho_5) + V(\lambda,\rho_6)]$, distortions caused by the influence of spectral characteristics of equipment are eliminated.

In experimental measurements, to determine the local spectral diffuse reflection coefficient $R(\lambda,\rho_k)$, it is necessary to know the spectral power density of the $\Phi_{\lambda S}(\lambda)$ flux introduced into the scattering medium under study, and the local density of diffuse reflection luminosity $M(\lambda,\rho_k)$. This requires determining the spectral dependencies $\Phi_{\lambda\text{HL}}(\lambda)$ and $\Phi_{\lambda\text{LED}}(\lambda)$ and mandatory calibration, i.e., determining the absolute spectral sensitivity of the equipment by the brightness of the radiation $S_L(\lambda) = L(\lambda)/V(\lambda)$ using a reference emitter (high-temperature blackbody model) [36,37]. Application of the traditionally used normalisation of the measured values $V(\lambda,\rho_k)$ to the normalising dependency $V_{Wnorm}(\lambda,\rho_0)$ obtained using a standard white reference reflector, i.e.,

$$V_{nW}(\lambda,\rho_k) = \frac{V(\lambda,\rho_k)}{V_{Wnorm}(\lambda,\rho_0)}, \tag{9}$$

allows us, with the subsequent multiplication of (9) by the factor $S_L(\lambda_m)/\Phi_{\mathrm{HL}}(\lambda_m)$, to obtain the absolute values of the local spectral diffuse reflection coefficient per unit solid angle Ω:

$$R_L(\lambda,\rho_k) = \frac{L(\lambda,\rho_k)}{\Phi_{\lambda\mathrm{HL}}(\lambda_m)} = \frac{S_L(\lambda_m)V_{nW}(\lambda,\rho_k)}{\Phi_{\lambda\mathrm{HL}}(\lambda_m)}, \tag{10}$$

since $V_{Wnorm}(\lambda_m,\rho_0) = 1$. Moreover, this normalisation takes into account the non-uniformity of the radiation spectrum of the source used, since the obtained values of $L(\lambda,\rho_k)$ are corrected and correspond to the brightness when using a source with a uniform spectrum $\Phi_s(\lambda) = \Phi_{\mathrm{HL}}(\lambda_m) = \mathrm{const}$. Expression (10) makes it possible to use the values $S_L(\lambda)$ and $\Phi_{\mathrm{HL}}(\lambda)$ (or $\Phi_{\mathrm{LED}}(\lambda)$) determined in a narrow part of the spectrum near λ_m. To go from $R_L(\lambda,\rho)$ with the dimension $1/(\mathrm{cm}^2\cdot\mathrm{sr})$ to $R(\lambda,\rho)$ with the dimension $1/\mathrm{cm}^2$ or $1/\mathrm{mm}^2$, it is necessary to integrate the resulting dependencies of the spectral brightness of the radiation leaving the medium over the solid angle Ω within the upper hemisphere:

$$M(\lambda,\rho_k) = \int_0^{2\pi}\int_0^{\pi/2} L(\lambda,\rho_k,\Theta,\varphi)\cos(\Theta_{uh})d\Theta_{uh}d\varphi_{uh}. \tag{11}$$

In the case when the radiation leaving the medium has the same brightness in all directions, $L(\lambda,\rho_k,\Theta_{uh},\phi_{uh}) = L(\lambda,\rho_k) = \mathrm{const}$, i.e., corresponds to Lambertian emitters, by integrating (11) one can obtain the following expression:

$$M(\lambda,\rho_k) = \pi L(\lambda,\rho_k). \tag{12}$$

Then, the local reflection coefficient is expressed as follows:

$$R(\lambda,\rho_k) = \frac{M(\lambda,\rho_k)}{\Phi_{\lambda\mathrm{HL}}(\lambda_m)} = \frac{k_M}{1-r_{tr}(\lambda)}\frac{\pi S_L(\lambda_m)V_{nW}(\lambda,\rho_k)}{\Phi_{\lambda\mathrm{HL}}(\lambda_m)}, \tag{13}$$

where k_M is a factor that takes into account the effect of the state of the sample surface (glossy or rough) on the obtained values of $R_m(\lambda,\rho_k)$, and r_{tr} is the reflection coefficient of the input radiation directly from the sample surface (specular component), which can be written as follows:

$$r_{tr}(\lambda) = \frac{[n_{sm}(\lambda)-1]^2 + \chi_{sm}^2(\lambda)}{[n_{sm}(\lambda)+1]^2 + \chi_{sm}^2(\lambda)}, \tag{14}$$

where $n_{sm}(\lambda)$ is the real part of the complex spectral refractive index of the sample $\widetilde{n}_{sm} = n_{sm} - i\chi_{sm}$, and $\chi_{sm}(\lambda) = \mu_a(\lambda)\cdot[\lambda/(4\pi)]$ is the imaginary part.

It should be noted that for scattering media with a glossy surface and small reduced scattering coefficients μ'_s, the condition of invariance of brightness $L(\Theta_{uh}) = \mathrm{const}$ for the angle Θ_{uh} may not be fulfilled due to the influence of the phenomenon of total internal reflection at angles of incidence $\Theta > \Theta_C$, and the factor k_M in (13) will be less than 1.

The recorded spectral–spatial profiles $R_m(\lambda,\rho_k)$ contain the necessary information to determine the spectral dependence $\mu_a(\lambda)$ when specifying the dependence $\mu'_s(\lambda)$ and parametric representation of the relationship between μ_a and μ'_s in the form of $\mu_a(\mu'_s)$. Indeed, by simulating the spectral dependencies $\mu_a(\lambda)$ и $\mu'_s(\lambda)$, and by using their parametric representation $\mu_a(\mu'_s)$ to construct the three-dimensional dependencies $R[\mu_a(\mu'_s),\rho_k]$ in a parametric form, shown in Figure 3 by bold coloured lines, one can make sure that each of them lies in its own plane of dependencies $R[\mu'_s,\mu_a,\rho_k]$ with the corresponding value of ρ_k. The noted properties of $R[\mu_a(\lambda),\mu'_s(\lambda),\rho_k]$ make it possible to propose a method for studying the applicability of the diffusion approximation models under consideration in diffuse reflection spectroscopy with a spatial resolution, which is based on fitting the varied simulated dependencies $R[\mu^*_a(\lambda),\mu'^*_s(\lambda),\rho_k]$ to the dependencies $R_m[\lambda,\rho_k]$ measured experimentally and on using the difference in the behaviour of the spectral dependencies $\mu'_s(\lambda)$ and $\mu_a(\lambda)$.

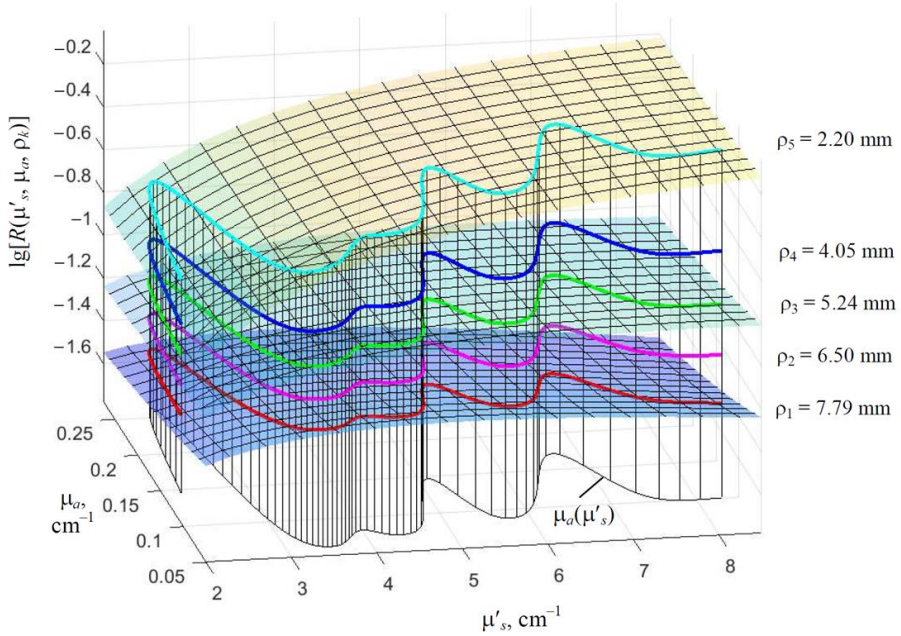

Figure 3. Dependencies lg[$R(\mu'_s,\mu_a,\rho_k)$] calculated for diffusion approximation model [14] and modelled dependencies lg{$R[\mu_a(\mu'_s)],\rho_k$} (bold coloured lines) at their parametric representation, illustrating that each of them is located within its plane of ρ_k values.

The fitting of the parameters of the diffusion approximation used in order to bring the varied simulated dependencies as close as possible to those measured experimentally was carried out by forming the corresponding residual function and minimising it by the least squares method using the Levenberg–Marquardt algorithm.

The spectral reduced scattering coefficient $\mu'_s(\lambda)$ usually increases smoothly with decreasing wavelength, and the spectral absorption index $\mu_a(\lambda)$ increases mainly in the absorption bands of the molecules included in the finely dispersed material under study, i.e., $\mu_a(\lambda)$ has a resonant character. Therefore, as noted above, when forming the variable spectral dependency $\mu'^*_s(\lambda)$, it is advisable to use the following hyperbolic dependency:

$$\mu'^*_s(\lambda) = \mu'^*_s(\lambda_0) \cdot (\lambda_0/\lambda)^{m^*_\lambda}, \tag{15}$$

where $\mu'^*_s(\lambda_0)$ is the variable value of the reduced scattering coefficient at wavelength λ_0, and m^*_λ is the variable exponent of the hyperbola degree λ_0/λ. This expression reduces to a power hyperbolic function $\mu'^*_s(\lambda) = a_0 \cdot \lambda^{-m^*_\lambda}$ depending on only two parameters, a_0 and m^*_λ. For the convenience of interpretation of $\mu'^*_s(\lambda)$, the article uses Formula (15), since the given value of the wavelength λ_0 allows one to locate a point with a unit value of the ratio λ_0/λ in the selected region of the wavelength scale. Note that the real dependencies $\mu'_s(\lambda)$ in a wide range of the spectrum may differ from (13), despite the good flexibility of this expression when varying $\mu'^*_s(\lambda)$. Therefore, in practice, more complex dependencies than (15) may be required.

Since the possibility of using the diffusion approximation has already been confirmed by Monte Carlo simulations and experimental measurements [14,15,18,23,24], it is inappropriate to repeat them. Therefore, in our studies, we used samples of several of the most common finely dispersed materials, consisting of a homogeneous matrix with filler particles embedded in it. Their spectral dependencies $\mu'_s(\lambda)$ and $\mu_a(\lambda)$ were unknown.

At the first stage of the applied method, the normalised dependencies $V_{nW}(\lambda_i,\rho_k)$ (9) are calculated from the obtained spectral dependencies $V(\lambda_i,\rho_k)$. After that, using (13), an experimentally measured spectral–spatial profile of the local diffuse reflection coefficient $R_m(\lambda,\rho_k)$ is formed.

When calibrating the equipment used according to the method described in [36,37], it was found that the sensitivity of the spectrometer in terms of the spectral brightness density L at λ_m = 658.4 nm is $S_L(\lambda_m) = 4.72 \times 10^{-7}$ W·ms/(cm^2·sr·μm). The power spectral density of the flux measured by calibrated spectrometer from the end of the optical fibre of the emitting probe when using a halogen lamp turned out to be equal to $\Phi_{\lambda HL}(\lambda_m) = 4.46 \times 10^{-3}$ W/μm. When studying samples of scattering media with a glossy surface, small values of μ'_s, and with the brightness of the diffusely reflected radiation, which depends on the angle Θ_{uh}, i.e., $L(\Theta_{uh}) \neq$ const, the coefficient $k_M < 1$, was used in front of the factor π in (13), which is necessary when taking into account the decrease in the luminosity M of the surface due to the effect of reflection from the interface of the light radiation both introduced into the medium and scattered by it.

At the second stage, the spectral–spatial profile $R\{\mu^*{}_a[\mu'^*{}_s(\lambda)],\rho_k\}$, modelled using the diffusion approximation, was fitted to the experimentally measured profile $R_m(\lambda,\rho_k)$ by varying the parameters $\mu'^*{}_s(\lambda)$ (15) and minimising the residual function.

The key point in compiling the residual function is the calculation of variable dependencies $\mu^*_a(\lambda_i,\rho_k)$, which depend on the applied diffusion approximation model and the specified variable dependency $\mu'^*{}_s(\lambda)$. As can be seen from Figure 3, for this, one can use pre-calculated planes of dependencies $R(\mu'_s, \mu_a, \rho_k)$, where the values of ρ_k correspond to the values used in experimental measurements. Then, using the function of numerical two-dimensional interpolation F_{2D} on a non-uniform sampling grid $R_m(\lambda_i,\rho_k)$, $\mu'^*{}_s$, it is possible to calculate the required family of variable spectral dependencies:

$$\mu^*_a(\lambda_i,\rho_k) = F_{2D}\left[R\left(\mu'_s,\mu_a,\rho_k\right),\mu'_s,\mu_a,R_m(\lambda_i,\rho_k),\mu'^*_s(\lambda_i)\right]. \quad (16)$$

This makes it possible to form the residual function for the measurement scheme used in the following form:

$$f_{R,\lambda}\left[\mu'^*_s(\lambda_0),m^*_\lambda,\lambda_i\right] = \sum_{k=1}^{5}\left\{\left[\frac{R\left[\mu'^*_s(\lambda_i),\mu^*_a(\lambda_i),\rho_k\right]}{R_m(\lambda_i,\rho_k)}-1\right]^2+\left[\frac{R\left[\mu'^*_s(\lambda_i),\mu^*_a(\lambda_i),\rho_{k+5}\right]}{R_m(\lambda_i,\rho_{k+5})}-1\right]^2\right\}, \quad (17)$$

Which, in numerical representation, is an array containing ten columns with the number of elements in each, determined by the number of readings of wavelengths λ_i in the spectrum range used in the calculations. This approach reduces the fit of the simulated variable dependencies $R\{\mu^*{}_a[\mu'^*{}_s(\lambda_i)],\rho_k\}$ to the experimentally measured $R_m(\lambda_i,\rho_k)$, i.e., minimisation of the residual function by varying only two parameters $\mu'^*{}_s(\lambda_0)$ and $m^*{}_\lambda$.

With a good agreement in the process of minimisation of (17) of all ten spectral dependencies $\mu^*_a(\lambda_i,\rho_k)$ obtained as a result of fitting with each other, it can be stated that the diffusion approximation is valid in a wide range of the spectrum for the ρ_k set of values used. When visualising the position of the minimum for the dependencies of the residual function values summed over λ_i, one can use the square root of the total residual function as follows:

$$\sigma_{R,\Delta\mu_a}\left[\mu'^*_s(\lambda_0),m^*_\lambda\right] = \sqrt{\sum_{\lambda_i}\left\{f_{R,\lambda}\left[\mu'^*_s(\lambda_0),m^*_\lambda,\lambda_i\right]\right\}}. \quad (18)$$

Modelling the fitting process with the addition of normal noise to the generated dependencies $R_m(\lambda_i,\rho_k)$ shows that the residual function used has a global minimum, so the resulting values $\mu'_s(\lambda_0)$ and m_λ with a good signal-to-noise ratio are determined quite accurately, i.e., have little spread.

There are three groups of sources of uncertainty that affect the results of determining the estimates $\mu'^*{}_s(\lambda_i)$ и $\langle\mu^*{}_a(\lambda_i,\rho_k)\rangle$, which are determined by the following:

(1) Heterogeneity and a priori uncertainty of the properties of the sample under study;
(2) Time instability of the parameters of the spectral equipment used and the unevenness of its spectral power density of the total noise;
(3) Limitations inherent in the applied diffusion approximation and the method for determining the desired dependencies $\mu'^*{}_s(\lambda_i)$ and $\langle\mu^*{}_a(\lambda_i,\rho_k)\rangle$.

Spatial averaging of the recorded spectral–spatial profiles of the local diffuse reflection coefficient $R_m(\lambda_i,\rho_k)$ will be effective in the presence of inhomogeneity of both the surface of the investigated sample and its properties. For example, averaging will have to be used with uneven mixing of the components of the sample under study at the stage of its production.

Note that the presence of surface inhomogeneity of the sample under study, radiation noise, and intrinsic noise of the spectrometer linear CCD array, as well as the deterioration of the signal-to-noise ratio of the recorded spectra at the edges of the spectral range used, limit the possibilities of the proposed technique. Therefore, in the process of research, it is necessary to choose a spectral range in which the dependencies of the resulting deviations of the obtained dependencies $\mu_a^*(\lambda,\rho_k)$ from their average value $\langle\mu_a^*(\lambda,\rho_k)\rangle$ were approximately the same over the entire spectrum. In some cases, when this cannot be achieved, it is necessary to refine the position of the wavelength λ_0 used so that the deviations $\mu_a^*(\lambda,\rho_k) - \langle\mu_a^*(\lambda,\rho_k)\rangle$ are more uniform.

The uncertainty of the used values of the effective coefficient of internal reflection into the rear hemisphere of the radiation R_{eff} that falls on the interface when leaving the medium requires separate consideration. The authors of [15,35,38] point out that the expression for this coefficient used in [14,18] gives a somewhat underestimated value of it, since photons approaching the boundary at small angles relative to the surface are mainly reflected back into the medium, and their concentration near the surface increases with increasing ρ compared to calculations based on the diffusion approximation. Therefore, if the dependencies coincide poorly with each other, it is necessary to investigate the influence of the used value of this coefficient R_{eff} on the deviations $\mu_a^*(\lambda,\rho_k)$ for the applied set of values ρ_k. In this case, it is necessary to accurately determine the refractive index of the medium n_{sm} [39].

The spectral resolution of modern portable spectrometers based on concave diffraction gratings and linear CCD arrays is sufficient for the problem under consideration [36,40,41], since the absorption spectra of condensed media are smooth, in contrast to the spectra of gases. The presence of instability of the parameters of the equipment used, radiation noise, and intrinsic noise of the spectrometer linear CCD array, as well as the deterioration of the signal-to-noise ratio of the recorded spectra at the edges of the spectral range used, limits the possibilities of the proposed method. Therefore, in the process of research, it is necessary to choose a spectral range in which the dependencies of the resulting deviations of the obtained dependencies $\mu^*{}_a(\lambda,\rho_k)$ on their average value $\langle\mu^*{}_a(\lambda,\rho_k)\rangle$ were approximately the same over the whole spectrum. In some cases, when this cannot be achieved, it is necessary to refine the position of the used wavelength λ_0 so that the deviations $\mu^*{}_a(\lambda,\rho_k)$–$\langle\mu^*{}_a(\lambda,\rho_k)\rangle$ are more uniform.

The fulfilment of the requirements, determined by the limitations of the diffusion approximation $\mu'_s(\lambda) >> \mu_a(\lambda)$ and $\sqrt{3\mu_a[\mu'_s + \mu_a]} \cdot \rho > 0.7$, is carried out by the correct choice of sample parameters and the ρ_k set of values used. A noticeable effect on the results of determining $\mu'^*{}_s(\lambda_i)$ and $\langle\mu^*{}_a(\lambda_i,\rho_k)\rangle$ can cause a deviation (in the short-wavelength part of the spectrum range used) of the real dependence $\mu'_s(\lambda)$ from the approximation used (15). Therefore, it is necessary to check the coincidence of the dependencies $\mu'^*{}_s(\lambda_i)$ obtained during fitting when the short-wave boundary of the spectrum range used is shifted to the right.

Since there is a significant number of terms and their designations in the article, Appendix A provides a list of them, which facilitates the perception and interpretation of the results.

5. Results of Experimental Investigation

To conduct experimental studies of the applicability of the diffusion approximation, the four samples of solid scattering structural materials were selected: 1—polyurethane with the addition of a red filler, 2—polyethylene terephthalate (caprolon) with a slight yellowish tinge, 3—white fluoroplastic, and 4—food grade white polystyrene. They were ranked according to the criterion of increasing the reduced scattering coefficient μ'_s, aver-

aged in the visible region of the spectrum. The surfaces of samples 2 and 4 were smoothed by grinding until a glossy sheen appeared in order to reduce the effect of its inhomogeneity on the obtained dependencies $R_m(\lambda,\rho_k)$. The ends of the more elastic cylindrical samples 1 and 3 were machined on a lathe with a flat cutter to obtain a smooth, diffusely scattering surface.

A narrow beam of light radiation, when it enters a strongly scattering medium, immediately loses its directionality since the scattering is multiple. Therefore, the authors of the diffusion approximation models under consideration [14,17,23] replace the directed radiation beam with a point emitter located at a depth z_0, as shown in Figure 1b. The loss of radiation directivity leads to a rapid decrease in its intensity with distance r compared to a transparent medium, since the radiation is scattered in all directions, and its intensity is described by Green's diffusion function (2). This leads to a rapid decrease in the local reflection coefficient $R(\rho)$, which makes it possible to apply the diffusion approximation to samples of scattering media with finite dimensions. Indeed, the effect of weak scattered radiation reflected back by the sample boundaries on the results of measurements of $R_m(\rho)$ at small used values of $\rho < 1$ cm turns out to be vanishingly small.

When processing the experimentally obtained spectral–spatial profiles using the above-described technique, it was found that approximation [17] describes the experimental dependencies much worse than those in [14] and [23]. Therefore, below are the results of processing using approximation [14], since approximation [23] was developed for biological tissues with $g \approx 0.8$ and small values of ρ. For small values of the anisotropy factor g, the results of applying [23] are approximately the same as for [14].

As expected, the inhomogeneity of the surface leads to differences in the experimental dependencies $R_m(\lambda_i,\rho_k)$, which are obtained to the left and right of the fixed probe. Basically, these differences cause a small parallel shift of the dependencies $R_m(\lambda_i,\rho_k)$ relative to each other, since the recorded fluxes depend on the surface state at each point ρ_k. This behaviour of $R_m(\lambda_i,\rho_k)$ influences the minimisation of the deviation of the spectral dependencies of the local diffuse reflection coefficient $R\{\mu^*{}_a[\mu'^*{}_s(\lambda_i)],\rho_k\}$ from the experimentally measured ones and causes a shift along the y-axis of estimates of the spectral dependencies $\mu^*{}_a(\lambda_i)$ obtained by fitting using (17).

It has been established that it is necessary to carefully choose the set of distances ρ_k used between emitting and receiving probes in order to satisfy the conditions of applicability of the diffusion approximation, for example, $\mu_{\text{eff}}\cdot\rho < 0.7$. On the one hand, at small values of ρ_k, there is a rapid increase in the positive deviation of the experimentally determined values $R_m(\lambda_i,\rho_k)$ from the simulated ones. On the other hand, for values $\rho_k > 0.6$ cm, there is also a gradual increase in the positive deviation of the measured dependencies $R_m(\lambda_i,\rho_k)$ from the simulated ones, which may be due both to the shortcomings of taking into account the effect of internal reflection of radiation by the surface of the medium, and to a small deviation axis of the movable probe from the vertical position.

The noted features are clearly manifested in the dependencies obtained by processing the experimentally obtained spectral–spatial profiles of $R_m(\lambda_i,\rho_k)$. Figure 4a shows the $R_m(\lambda_i,\rho_k)$ dependencies for sample 1 in a semi-logarithmic scale obtained with the moving probe positioned to the left (L) (solid colour lines) and to the right (R) (solid thin black lines) of the stationary probe. The dashed lines (coloured and black, respectively) show the fitting results. When calculating the variable dependence $\mu'^*{}_s(\lambda_i)$ (15), the wavelength $\lambda_0 = 955$ nm was chosen in the region of the local minimum of the total attenuation of radiation by the medium of this sample. The spectral dependencies $\mu'^*{}_s(\lambda)$ and $\mu^*{}_a(\lambda,\rho_k)$ obtained as a result of fitting are shown in Figure 4b with a bold red line and a thin coloured line, respectively. The average dependency $\overline{\mu}^*_{a2,9}(\lambda_i) = [\mu^*_a(\lambda_i,\rho_2) + \mu^*_a(\lambda_i,\rho_9)]/2$ is shown with a bold magenta line.

This polyurethane sample was sufficiently elastic, so that its surface did not have a glossy sheen, and the nature of the diffusely scattered radiation emerging from it approximately corresponded to that of Lambert. Therefore, the coefficient k_M was assumed to be equal to 1 for it when fitting the spectral dependencies. The presence of a red filler in this

sample affected the behaviour of the measured spectral–spatial profile of $R_m(\lambda_i,\rho_k)$ in the visible region of the spectrum. The absorption of radiation by the filler particles caused a significant dip in the spectral–spatial profile of the local reflection coefficient, which is illustrated by the dependencies in Figure 4. Strong radiation absorption reduced the signal-to-noise ratio of the recorded spectral dependencies. Therefore, they were pre-smoothed with a digital Savitzky–Golay filter in order to visually improve their appearance at the short- and long-wavelength decreases in the spectral sensitivity of the equipment used.

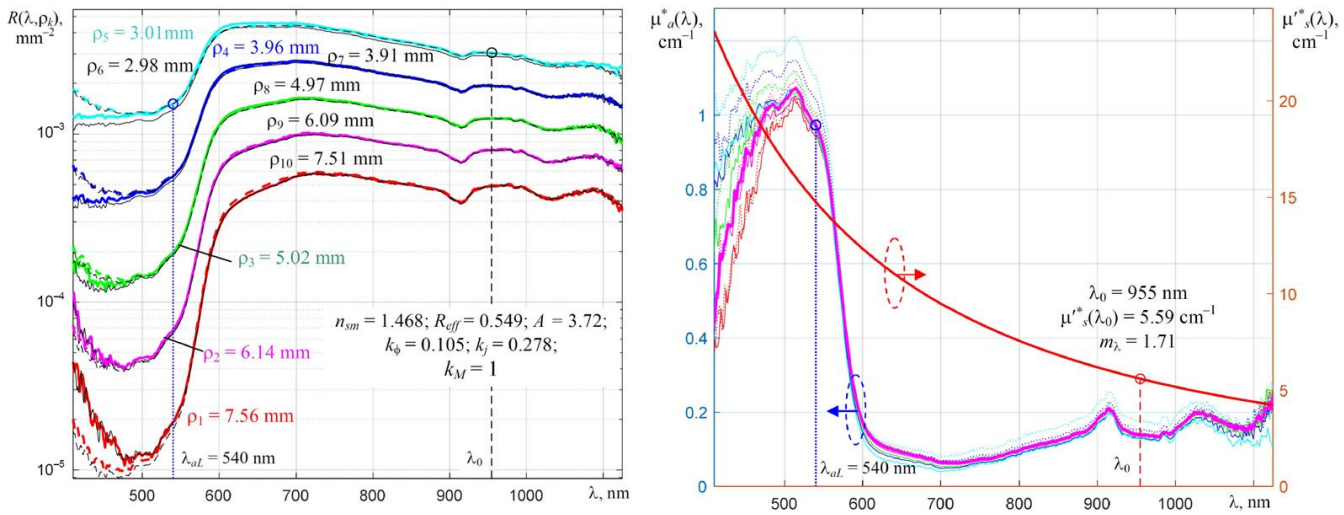

Figure 4. Families of dependencies of the measured spectral local reflection coefficient $R_m(\lambda_i,\rho_k)$ (solid coloured lines (when the movable probe is positioned on the left L from the emitter) and black lines (when it is positioned to the right R)) and dependencies, obtained by fitting $R\{\mu^*_a[\mu'^*_s(\lambda_i)],\rho_k\}$ (dashed coloured and black lines, respectively) (**a**), and dependencies of spectral coefficients of reduced scattering $\mu'^*_s(\lambda_i)$ (bold red line) and absorption $\mu^*_a(\lambda_i,\rho_k)$ (coloured continuous lines for L and dotted lines for R) (**b**) for sample 1 at different values of ρ_k.

The surface roughness of sample 1 reduces the effect of internal reflection. Therefore, as can be seen from Figure 4a, the fitted dependencies in the spectrum range from λ_{aL} = 540 nm to λ_{aL} = 1100 nm agree well with the experimentally measured values of $R_m(\lambda,\rho_k)$. The verification of the fulfilment of the condition for the applicability of the diffusion approximation $\mu^*_{\text{eff}}\cdot\rho_k \geq 0.7$ for the set of values ρ_k used showed that it is partly not met only for the two smallest distances ρ_k between the probes in the long-wavelength part of the spectrum.

The surface of the second, less elastic caprolon sample had a glossy sheen; therefore, the value of the coefficient k_M when fitting the spectral dependencies was chosen to be 0.72. This sample exhibits a noticeable absorption of radiation in the region of the spectrum corresponding to the blue colour, which is illustrated by the spectral dependencies in Figure 5. Two pronounced absorption bands of the matrix of this finely dispersed material appear in the infrared region of the spectrum. At two minimum distances between the probes ρ_k, the condition of applicability for the diffusion approximation $\mu^*_{\text{eff}}\cdot\rho_k \geq 0.7$ is also partly not satisfied.

This sample exhibits a larger spread of the fitted dependencies $\mu^*_a(\lambda,\rho_k)$ and noticeable deviations of the dependencies $R\{\mu^*_a[\mu'^*_s(\lambda_i)],\rho_k\}$ from the experimentally obtained ones $R_m(\lambda_i,\rho_k)$. Moreover, the values $R_m(\lambda_i,\rho_k)$ obtained for the extreme points ρ_k turn out to be slightly larger than $R\{\mu^*_a[\mu'^*_s(\lambda_i)],\rho_k\}$ obtained as a result of the fitting.

The noted deviations are more clearly manifested in the corresponding dependencies for the white fluoroplastic (3rd sample), which are shown in Figure 6. For it, the applicability condition for the diffusion approximation $\mu^*_{\text{eff}}\cdot\rho_k \geq 0.7$ was fulfilled for all used values of ρ_k.

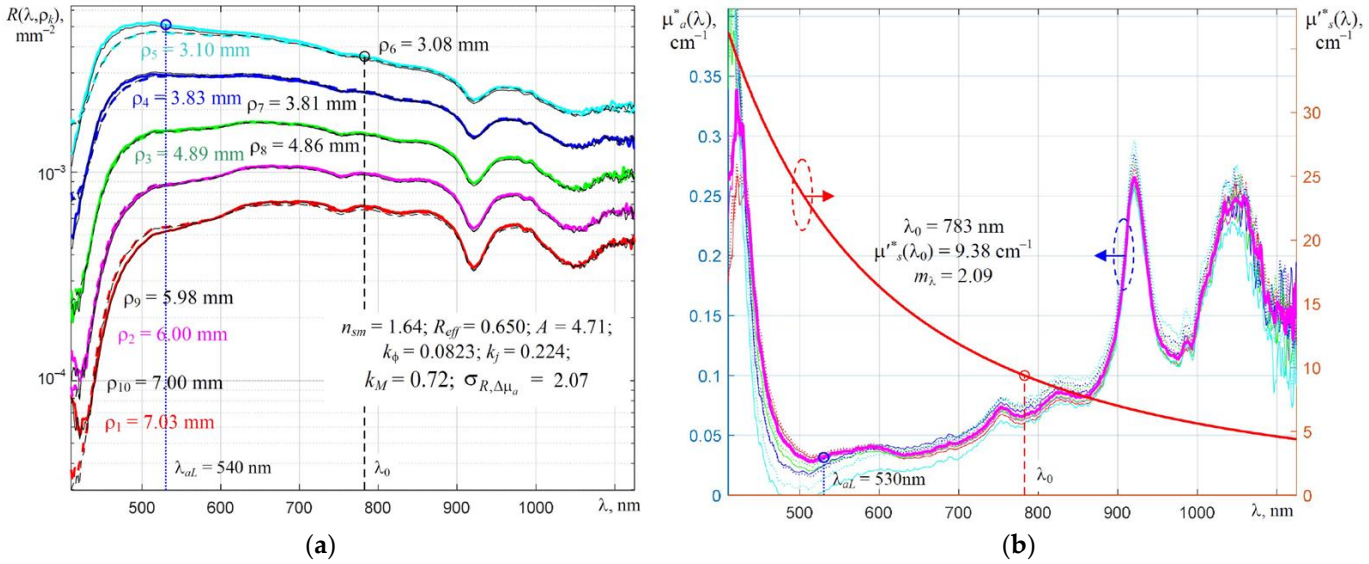

Figure 5. Families of dependencies of the measured spectral local reflection coefficient $R_m(\lambda_i,\rho_k)$ (solid coloured lines (when the movable probe is positioned on the left L from the emitter) and black lines (when it is positioned to the right R)) and dependencies, obtained by fitting $R\{\mu^*_a[\mu'^*_s(\lambda_i)],\rho_k\}$ (dashed coloured and black lines, respectively) (**a**), and estimates of spectral coefficients of reduced scattering $\mu'^*_s(\lambda_i)$ (bold red line) and absorption $\mu^*_a(\lambda_i,\rho_k)$ (coloured continuous lines for L and dotted lines for R) (**b**) for sample 2 at different values of ρ_k.

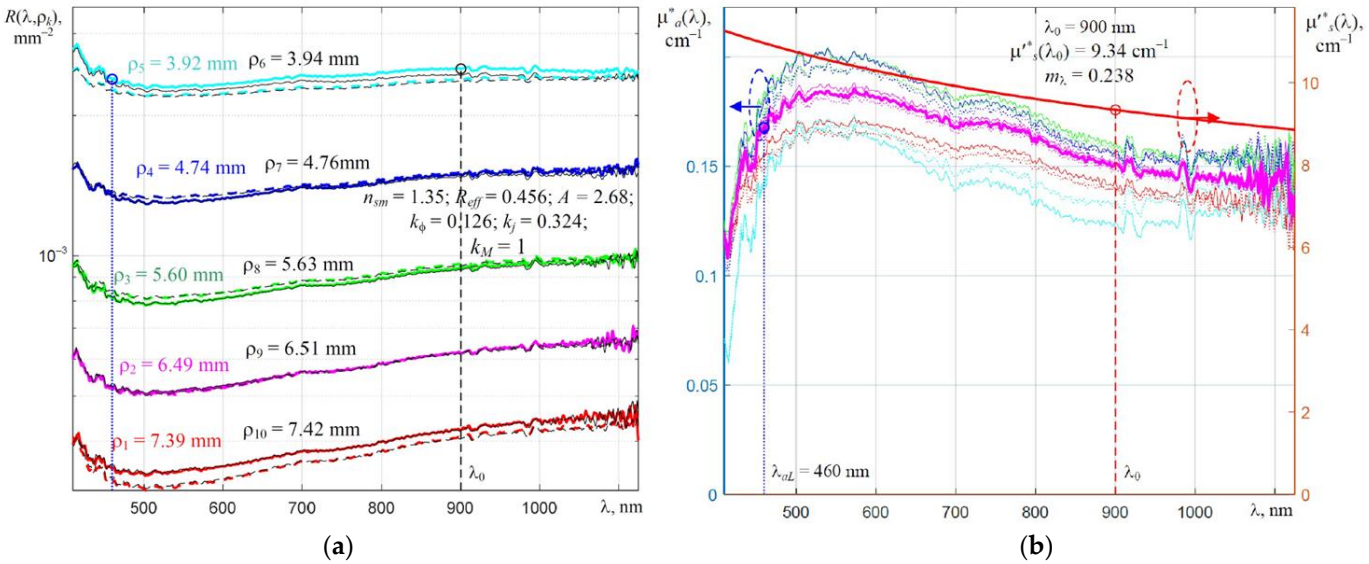

Figure 6. Families of dependencies of the measured spectral local reflection coefficient $R_m(\lambda_i,\rho_k)$ (solid coloured lines (when the movable probe is positioned on the left L from the emitter) and black lines (when it is positioned to the right R)) and dependencies, obtained by fitting $R\{\mu^*_a[\mu'^*_s(\lambda_i)],\rho_k\}$ (dashed coloured and black lines, respectively) (**a**), and estimates of spectral coefficients of reduced scattering $\mu'^*_s(\lambda_i)$ (bold red line) and absorption $\mu^*_a(\lambda_i,\rho_k)$ (coloured continuous lines for L and dotted lines for R) (**b**) for sample 3 at different values of ρ_k.

The inhomogeneity of the surface of the sample under investigation, the presence of noise and distortions of the recorded spectral–spatial profiles, as well as their real shape, affect the uniqueness of the solutions obtained. In the presence of changes in the absorption index $\mu_a(\lambda)$ in the short-wavelength part of the spectrum range used, the global minimum of the residual function (18) is quite clearly pronounced. The foregoing is well illustrated by the dependency $\sigma_{R,\Delta\mu_a}\left[\mu'^*_s(\lambda_0), m^*_\lambda\right]$ for sample 1, shown in Figure 7a. In order to

improve the visual perception of the presence of secondary local minima in a wide range of $\mu'^*_s(\lambda_0)$ and m^*_λ values, when forming (18) and constructing the surface $\sigma_{R,\Delta\mu_a}\left[\mu'^*_s(\lambda_0), m^*_\lambda\right]$, the square root was extracted from the sum of the squares of the components of the residual function. Additionally, when forming this surface, the limitation of $\sigma_{R,\Delta\mu_a}$ values was used, so a flat area is observed on it. For sample 1, the solution point shown in Figure 7a with a red circle is quite stable and weakly depends on the shift of the short-wavelength boundary λ_{aL} of the spectral range used in the fitting.

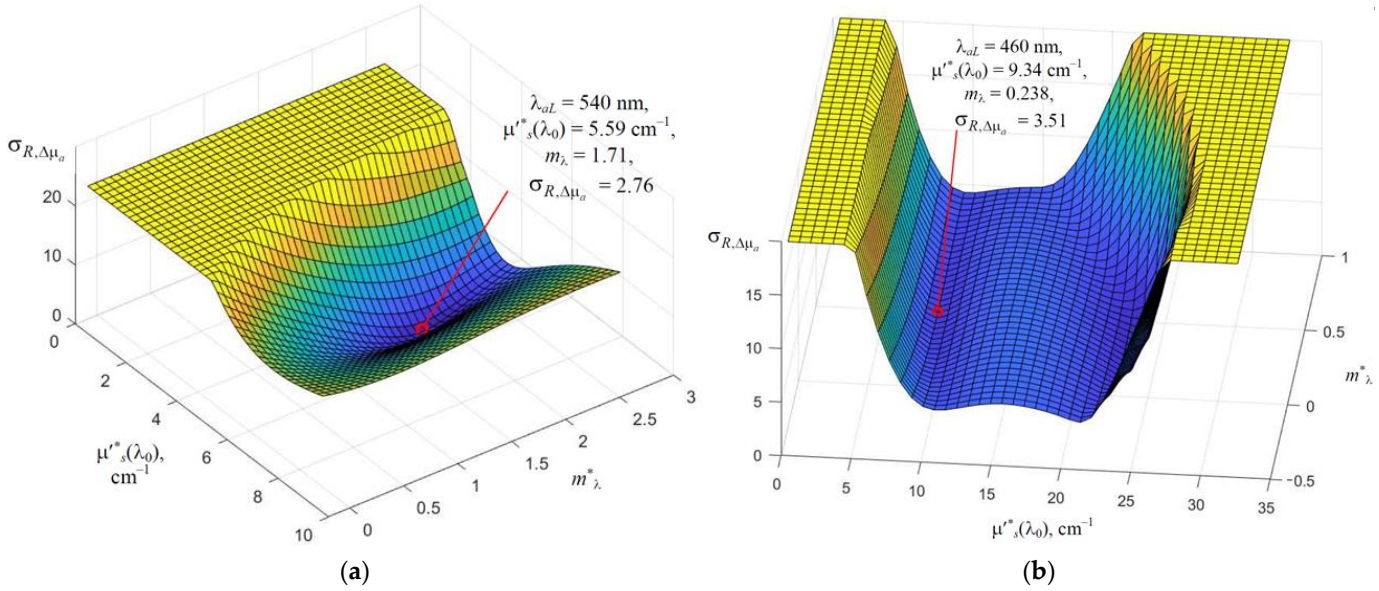

(**a**) (**b**)

Figure 7. Calculated dependency of the square root of the function of residual $\sigma_{R,\Delta\mu_a}\left[\mu'^*_s(\lambda_0), m^*_\lambda\right]$ on $\mu'^*_s(\lambda_0)$ and m^*_λ for sample 1 (**a**) for initial data presented in Figure 3 and for sample 3 (**b**) for initial data presented in Figure 6.

With a monotonic dependency $\mu_a(\lambda)$, the resulting spectral–spatial profile is formed by smooth changes in the spectral dependencies $\mu'_s(\lambda)$ and $\mu_a(\lambda)$. Therefore, when fitting, there can be several solutions, i.e., local minima of the dependency $\sigma_{R,\Delta\mu_a}\left[\mu'^*_s(\lambda_0), m^*_\lambda\right]$. The corresponding dependency calculated for sample 3 is shown in Figure 7b. One can see that in such cases, when carrying out the fitting, it is necessary to check whether the obtained solution falls into the unacceptable range of $\mu'^*_s(\lambda)$ and m^*_λ values. With smooth changes in $\mu_a(\lambda)$, the dependency of $\sigma_{R,\Delta\mu_a}\left[\mu'^*_s(\lambda_0), m^*_\lambda\right]$ on m^*_λ becomes weak, since such a monotonous change is formed by a decrease in the values of $\mu^*_a(\lambda)$, a gradual increase in $\mu'^*_s(\lambda)$, and a simultaneous change in the slope of $\mu'^*_s(\lambda)$ by decreasing the value of m^*_λ. This behaviour of $\sigma_{R,\Delta\mu_a}\left[\mu'^*_s(\lambda_0), m^*_\lambda\right]$ for sample 3 is well illustrated by the dependency in Figure 7b. Along the m^*_λ axis, the $\sigma_{R,\Delta\mu_a}$ value changes slightly, and the minimum is much less pronounced than along the $\mu'^*_s(\lambda_0)$ axis.

There are also two points of local minima, which are located at the bottom of two adjacent ravines. The second point with a large value of $\mu'^*_s(\lambda_0)$ was discarded since, for it, a significant part of the obtained dependencies $\mu^*_a(\lambda)$ turns out to be less than zero, which is not true. The first point with a smaller value $\mu'^*_s(\lambda_0)$ is taken as a solution and is used in plotting the dependencies in Figure 6b.

Distortions of the recorded spectral–spatial profiles lead to greater uncertainty in the solutions obtained. In the short-wavelength part of the spectral dependencies for the second and fourth samples, the influence of parasitic radiation is manifested, which is scattered by the concave diffraction grating of the spectrometer into the zero order of diffraction. This effect was revealed by us earlier when calibrating AvaSpec 2048WL and C12880MA Hamamatsu spectrometers according to reference emitters with different temperatures [37,40,41]. The halo maximum of weak radiation scattered by the concave

diffraction grating of the AvaSpec 2048WL spectrometer to zero order is located in the area that corresponds to diffracted blue radiation. This scattered radiation is added to the diffracted one, which causes a significant distortion (overestimation) of the spectral $R_m(\lambda_i,\rho_k)$ in the visible region. For the absorption bands of the material of sample 4 in the infrared region of the spectrum, there is no such shift; therefore, the fitted $R(\lambda_i,\rho_k)$ and measured $R_m(\lambda_i,\rho_k)$ dependencies in Figure 8a, as well as $\mu^*_a(\lambda)$ in Figure 8b, are close to each other in this region. Verification of the applicability condition for the diffusion approximation $\mu^*_{\text{eff}}\cdot\rho_k \geq 0.7$ for sample 4 showed that it is satisfied for all values of ρ_k used.

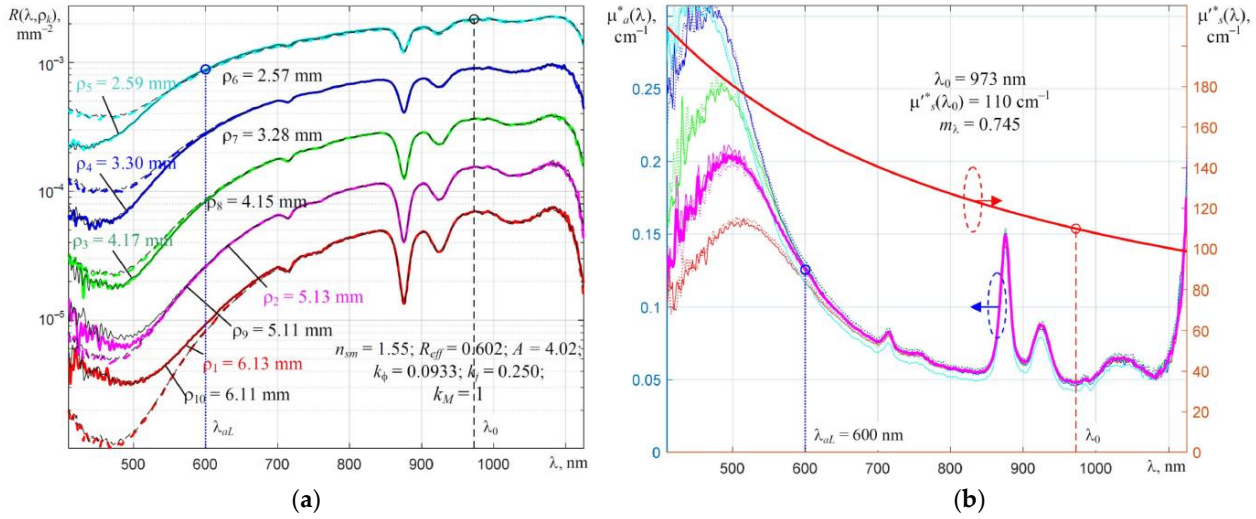

Figure 8. Families of dependencies of the measured spectral local reflection coefficient $R_m(\lambda_i,\rho_k)$ (solid coloured lines (when the movable probe is positioned on the left L from the emitter) and black lines (when it is positioned to the right R)) and dependencies, obtained by fitting $R\{\mu^*_a[\mu'^*_s(\lambda_i)],\rho_k\}$ (dashed coloured and black lines, respectively) (**a**), and estimates of spectral coefficients of reduced scattering $\mu'^*_s(\lambda_i)$ (bold red line) and absorption $\mu^*_a(\lambda_i,\rho_k)$ (coloured continuous lines for L position and dotted lines for R position) (**b**) for sample 4 at different values of ρ_k.

As can be seen from the comparison of dependencies in Figures 5 and 8, the influence of this effect is more clearly manifested for sample 4, in which the coefficients of reduced scattering $\mu'^*_s(\lambda)$ and radiation absorption $\mu_a(\lambda)$ in the visible region are greater than those of sample 2. Therefore, in comparison with sample 2, the contribution of radiation with $\lambda > 600$ nm, scattered to the zero order, for sample 4 is much larger, which leads to a strong distortion of $R_m(\lambda_i,\rho_k)$ in the visible region of the spectrum.

This forces the left boundary λ_{aL} of the spectral range used to be shifted to the right so that these distortions do not lead to a shift in the solution point for the fitted dependencies. When the boundary λ_{aL} is shifted to the point $\lambda_{aL} = 500$ nm, the noted distortions of the spectral–spatial profile lead to a slight shift of the solution point towards lower values of $\mu^*_s(\lambda_0)$ with a simultaneous increase in the value of m^*_λ to bring the simulated dependencies closer to the distorted ones.

Since in the fitted dependency $\mu^*_a(\lambda)$, the bands of absorption of radiation by polystyrene are visible, the global minimum of the dependency is quite pronounced, and the resulting solution is quite stable.

The opposite slopes of the spectral dependencies of the coefficient of local diffuse reflection of radiation $R_m(\lambda,\rho_k)$ for the first and second samples compared to the fourth sample in the near-infrared region of the spectrum are caused by the different behaviour of the spectral radiation absorption indices $\mu^*_a(\lambda)$ by these samples. For the first and second samples, the dependencies $\mu^*_a(\lambda)$ decrease, on average, with increasing λ, and for the fourth sample, on the contrary, they increase. Expression (5) for calculating $R(\lambda,\rho_k)$ includes the spectral radiation attenuation index $\mu_{\text{eff}}(\lambda) = \sqrt{3\mu_a(\lambda)[\mu_a(\lambda) + \mu'_s(\lambda)]}$, so the interaction $\mu_a(\lambda)$ and $\mu'_s(\lambda)$ determines the shape of the registered dependencies $R_m(\lambda_i,\rho_k)$. Elemen-

tary electric dipoles of particles of finely dispersed fillers introduced into the material matrix participate in the absorption of light radiation, which can lead to their significant contribution to the obtained dependencies of the calculated absorption index $\mu^*_a(\lambda)$.

It should be noted that living tissues differ from isotropically scattering materials by a strong structural inhomogeneity. Subcutaneous tissues have different structures and contain an extensive circulatory system. In the spectral range $\lambda < 600$ nm, haemoglobins contained in blood erythrocytes have a high radiation absorption index $\mu_a(\lambda)$. Therefore, the effect of parasitic radiation noted above, which is scattered by the concave diffraction grating of the spectrometer to zero order, also manifests itself in the obtained dependencies, which is illustrated by Figure 9.

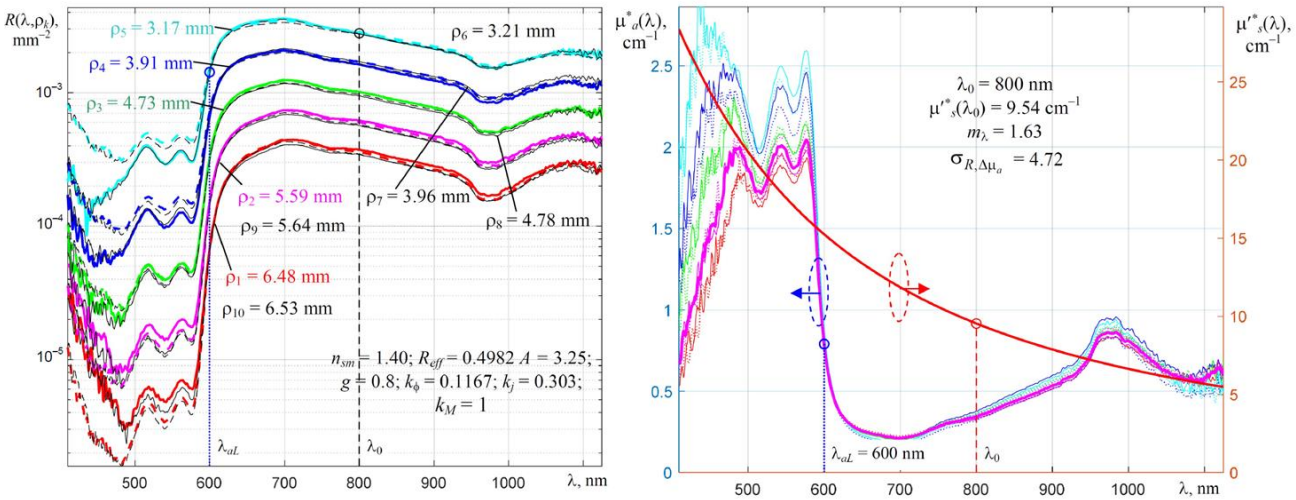

Figure 9. Families of dependencies of the measured spectral local reflection coefficient $R_m(\lambda_i,\rho_k)$ (solid coloured lines (when the movable probe is positioned on the left L from the emitter) and black lines (when it is positioned to the right R)) and dependencies, obtained by fitting $R\{\mu^*_a[\mu'^*_s(\lambda_i)],\rho_k\}$ (dashed coloured and black lines, respectively) (**a**), and estimates of spectral coefficients of reduced scattering $\mu'^*_s(\lambda_i)$ (bold red line) and absorption $\mu^*_a(\lambda_i,\rho_k)$ (coloured continuous lines for L position and dotted lines for R position) (**b**) for living tissue in the thenar region of the palm at different values ρ_k.

Since the diffusion approximation model [23] is intended for biological tissues, it is interesting to compare the results of applying models [14,23] for living blood-filled tissues. It is considered that for biological tissues, the anisotropy factor is $g = 0.8$, and the refractive index is $n_{sm} = 1.4$ [11]. Since the proposed method for estimating the spectral indices $\mu'^*_s(\lambda)$ and $\mu^*_a(\lambda)$ for media with $\mu'^*_s(\lambda) < 40$ cm^{-1} is applicable at distances between probes $\rho \geq 0.3$ cm, the spectral–spatial profiles of living blood-filled tissue in the region of the adductor muscle of the thumb (thenar) of the hand with a sufficient thickness of muscle tissue were measured. An example of the results of fitting this spectral–spatial profile of the local reflection coefficient $R\{\mu^*_a[\mu'^*_s(\lambda)],\rho_k\}$ to the experimentally obtained $R_m(\lambda,\rho_k)$ using approximation [14] is shown in Figure 9a. When using approximation [23], the corresponding dependencies are approximately the same.

Since the source of radiation was a halogen lamp and biological tissues weakly absorb radiation in the near-infrared region, the addition of parasitic infrared radiation, which is scattered by the diffraction grating in the zero order, leads to significant distortions of the fitted dependencies in the visible region of the spectrum, which is also illustrated by the dependencies in Figure 9. Therefore, to study the dependencies $\mu'^*_s(\lambda)$ and $\mu^*_a(\lambda)$ of living tissues in the visible region of the spectrum, it is necessary to use another radiation source instead of a halogen lamp, for example, a super bright white LED. Then, the contribution of radiation with a wavelength $\lambda > 600$ nm to the formed distortions will sharply decrease.

The total power of the main and auxiliary dipole sources of radiation introduced into the scattering medium for the approximation [23] must coincide with the power of the dipole source for approximation [14]. Therefore, due to the transfer of a part of the diffusely reflected light flux to the central peak of the diffuse reflection for approximation [23] in comparison with approximation [14], there is a slight decrease in the calculated local reflection coefficient $R(\rho)$ for $\rho_k > 1$ mm. Despite the coincidence of the fitted dependencies $R\{\mu^*_a[\mu'^*_s(\lambda_0)],\rho_k\}$ when using [14,23], the noted difference leads to a noticeable shift in the resulting spectral dependency $\mu'^*_s(\lambda)$ down and the corresponding shift of $\mu^*_a(\lambda)$ up when using [23] compared to [14]. Therefore, the possibility of using approximation [23] in diffuse scattering spectroscopy with a spatial resolution even at small distances ρ between the probes requires thorough additional study. Our estimate of the volumetric concentration of water in the thenar tissues from its absorption band with a maximum of about 970 nm gives a value of about 70% when using [14], which approximately corresponds to the physiological norm of muscle tissue hydration.

The inhomogeneity of the tissue in the thenar region, as shown in Figure 9b, leadsto approximately a twofold increase in the value of the global minimum of dependency $\sigma_{R,\Delta\mu_a}\left[\mu'^*_s(\lambda_0), m^*_\lambda\right]$ described by (18). In this case, the global minimum of the dependency becomes weakly pronounced along the m_λ axis. Therefore, when studying the dependencies $\mu'^*_s(\lambda)$ and $\mu^*_a(\lambda)$ of living tissues, it is necessary to carefully choose the studied point of the body so that the influence of the heterogeneity of the distribution in the small vessel compartment is minimal. It is also advisable to narrow the range of distances ρ_k used between the point of input of radiation into the tissue and the points of registration of diffusely scattered radiation. It is desirable that the thickness of the tissue is significantly greater than the maximum of the used values of ρ_k. This is observed for thenar, since the radiation is almost completely absorbed by the tissues of this area of the palm.

6. Discussion of the Research Results

The study of the applicability of the diffusion approximation in determining the spectral coefficients of reduced scattering $\mu'^*_s(\lambda)$ and absorption $\mu^*_a(\lambda)$ of radiation for four samples of solid scattering structural materials and living tissue in the thenar area of the palm made it possible to identify the main sources affecting the accuracy of estimates $\mu'^*_s(\lambda)$ and $\mu^*_a(\lambda)$ obtained when using diffuse reflectance spectroscopy with spatial resolution.

It is shown that at small values of $\mu'_s(\lambda)$ at the boundaries of the range of variation of the distance ρ_k between the probes, there are slight excesses of the experimentally obtained values of the coefficient of local diffuse reflection of radiation $R_m(\lambda,\rho_k)$ over the fitted $R\{\mu^*_a[\mu'^*_s(\lambda_0)],\rho_k\}$ ones using the diffusion approximation. These excesses manifest themselves at small distances ($\rho_k < 3$ mm) between the point of input of radiation into the scattering medium and the point of its registration, i.e., when the condition for the feasibility of the diffusion approximation $\mu_{\text{eff}}(\lambda)\cdot\rho_k > 0.7$ is violated [14]. Incomplete consideration of the processes of reflection of radiation from the interface between the media, as entered into the scattering medium, and leaving it, can also lead to a similar excess of the values of $R_m(\lambda,\rho_k)$ over the fitted values $R\{\mu^*_a[\mu'^*_s(\lambda_0)],\rho_k\}$ for a glossy surface and maximum values of ρ_k. Also, at small values of $\mu'^*_s(\lambda)$, a significant deviation of the diffuse reflection brightness distribution from the Lambert one can be observed, which requires a decrease in the value of the coefficient k_m. These deviations lead to a shift or a noticeable spread along the *y*-axis of the dependencies $\mu^*_a(\lambda,\rho_k)$, which are calculated in the process of fitting the varied spectral–spatial profiles of the local reflection coefficient $R\{\mu^*_a[\mu'^*_s(\lambda_i)],\rho_k\}$ to the experimentally determined $R_m(\lambda_i,\rho_k)$. In the presence of noted deviations, the set of distances ρ_k used between the probes should be optimised, which will reduce the spread $\mu^*_a(\lambda,\rho_k)$. If it is not possible to correct the boundaries of the range of variation of the set ρ_k used, it is necessary to use a correction function that should increase the concavity of the recorded dependencies $R_m(\lambda,\rho_k)$ along the ρ axis in order to reduce the shift of the obtained dependencies $\mu^*_a(\lambda,\rho_k)$ relatively to each other.

The inhomogeneity of the surface of the scattering medium, i.e., the presence of its roughness, also leads to a similar shift of the dependencies $\mu^*_a(\lambda,\rho_k)$ along the ordinate axis, which forces one to resort to averaging the recorded spectral–spatial profiles $R_m(\lambda,\rho_k)$ to reduce the spread of $\mu^*_a(\lambda,\rho_k)$.

In order to exclude the influence of the characteristics of the spectral equipment used on the shape of the determined spectral–spatial profile $R_m(\lambda_i,\rho_k)$, the normalisation of the recorded dependencies $V(\lambda_i,\rho_k)$ to the normalised spectrum of the reference white reflector with a maximum equal to unity, and the determination of the absolute spectral sensitivity of the equipment used by its calibration according to the reference emitter, should be conducted.

Distortions are revealed in the recorded spectral–spatial profiles of the local reflection coefficient $R_m(\lambda,\rho_k)$ in the visible region of the spectrum, which arise due to parasitic radiation scattered by a concave diffraction grating to zero order. These distortions are characteristic of compact spectrometers based on linear CCD arrays. Moreover, the maximum distortion is usually located in the region that corresponds to the dispersed blue radiation of the first-order diffraction. Therefore, if it is necessary to determine the spectral indices $\mu'_s(\lambda)$ and $\mu_a(\lambda)$ in the visible region of the spectrum, one must carefully choose the radiation source used so that its intensity in the infrared region of the spectrum would be less than in the visible region.

The possibility of using the diffusion approximation [23] in diffuse reflection spectroscopy with spatial resolution requires additional study, since the results of its use differ from the results obtained using the classical approximation [14].

It is necessary to add the error in determining the refractive index of the controlled material n_{sm} and the error in determining the local diffuse reflection coefficient $R_m(\lambda,\rho_k)$ to the sources of uncertainty listed above. Moreover, the accuracy of determining $R_m(\lambda,\rho_k)$ is determined by the calibration errors of the spectral equipment used, i.e., the absolute sensitivity $S_L(\lambda)$ and the measurement accuracy of the spectral flux $\Phi_\lambda(\lambda)$ introduced into the sample of the scattering medium under study, as well as the state of its surface.

To reduce the effect of spatial inhomogeneity on the properties of the sample under study, averaging of the recorded spectral–spatial profiles of diffuse reflection over its surface should be applied.

Thus, when using the registration of spectral–spatial profiles of diffuse reflection $R_m(\lambda,\rho_k)$ in a wide part of the spectrum, it is possible to increase the unambiguity of determining the spectral indices $\mu'^*_s(\lambda)$ and $\mu^*_a(\lambda)$, since the minimum of the residual function (16) becomes more pronounced. However, the shape of the spectral–spatial profile of the local diffuse reflection coefficient $R_m(\lambda,\rho_k)$ affects the unambiguity of the obtained dependencies $\mu'^*_s(\lambda)$ and $\mu^*_a(\lambda)$. This requires a mandatory check for the unambiguity of the solution. The proposed method for determining $\mu'^*_s(\lambda)$ and $\mu^*_a(\lambda)$ makes it possible to visualise the surface $\sigma_{R,\Delta\mu_a}\left[\mu'^*_s(\lambda_0), m^*_\lambda\right]$ and not consider incorrect results corresponding to the hit of the solution point $\mu'^*_s(\lambda_0)$,m_λ in a side local minimum.

It should be noted that standard spectral equipment for alternative verification of the reliability of the obtained spectral properties of the studied samples of scattering materials and living tissue is not commercially available. This fact must be considered as a limitation inherent in the study. Therefore, further efforts are needed to create appropriate spectral equipment and their standardisation.

The described possibilities of diffuse reflection spectroscopy in determining the optical properties of finely dispersed scattering media are attractive to manufacturers of optoelectronic equipment designed for the rapid determination and control of the spectral indices $\mu'_s(\lambda)$ and $\mu_a(\lambda)$ of various scattering materials, including living tissues. In the industry, such equipment can be required for operational control of composite materials at the stage of their production. With the optimal choice of the spectral parts used and the possibility of averaging the spectral–spatial profiles $R_m(\lambda,\rho_k)$, the discussed equipment can be used in agriculture, for example, for the rapid determination of the optical properties of milk and dairy products. The possibility of determining the dependencies $\mu'_s(\lambda)$ and $\mu_a(\lambda)$ in abso-

lute measure (with the dimensions of cm^{-1} or mm^{-1}) is attractive for operational control of the optical properties and volume concentration of the main chromophores of fruits and vegetables and their changes during storage. The potential capabilities of the appropriate equipment for determining hydration and the main parameters of the microcirculatory bed of the circulatory system of the body's tissues are attractive for assessing the condition of the skin in cosmetology and monitoring the treatment of burns, tissue oedema, and hypertension in medicine.

7. Conclusions

The proposed method for registering the spectral–spatial profiles of the local diffuse reflection coefficient $R(\lambda,\rho_k)$ of light radiation by scattering media and their further processing makes it possible to determine the spectral coefficients of reduced scattering $\mu'_s(\lambda)$ and absorption $\mu_a(\lambda)$ of radiation by these media under additional limiting conditions (namely, $\mu'_s(\lambda) >> \mu_a(\lambda)$, the monotonicity of the change $\mu'_s(\lambda)$ in the part of the spectrum used, and $\mu_{eff}(\lambda)\cdot\rho_k > 0.7$). The assessment of the possibility of using known diffusion approximations [14,17,23] showed that approximation [17] should not be used in determining $\mu'_s(\lambda)$ and $\mu_a(\lambda)$. The results of determining $\mu'_s(\lambda)$ and $\mu_a(\lambda)$ when applying approximation [23] to the recorded spectral–spatial profiles $R_m(\lambda,\rho_k)$ of a non-isotropic medium (living blood-filled tissue in the area of the thenar of the palm) differ from $\mu'_s(\lambda)$ and $\mu_a(\lambda)$ obtained using the classical approximation [14]. Therefore, to elucidate the possibility of using approximation [23], further thorough studies are required.

The sources of uncertainty of the obtained solutions are identified, and solutions are proposed to reduce their influence on the errors in determining the desired dependencies $\mu'_s(\lambda)$ and $\mu_a(\lambda)$. In order to improve the accuracy of determining the composition of optically active components of scattering media, it is important to expand the spectrum range used to the mid-infrared region, where the main vibrational–rotational absorption bands of radiation of various molecules are located.

The results of the study presented in the article will be useful for the developers of new small-sized optoelectronic equipment designed for non-destructive online control of the main optical characteristics of various finely dispersed scattering media, including living tissues. The potential for its practical application is extensive—from various applications in industry and agriculture to medical equipment for clarifying diagnostics.

Author Contributions: Conceptualisation, O.H. and V.F.; methodology, O.H., V.F. and K.S.; software, V.F. and K.S.; validation, K.S.; formal analysis, O.H. and V.F.; investigation, O.H., V.F., K.S. and P.K.; writing—original draft preparation, K.S. and P.K.; writing—review and editing, O.H. and V.F.; visualisation, K.S. and P.K.; supervision, V.F. All authors have read and agreed to the published version of the manuscript.

Funding: This research received no external funding.

Institutional Review Board Statement: Not applicable.

Informed Consent Statement: Not applicable.

Data Availability Statement: Not applicable.

Conflicts of Interest: The authors declare no conflict of interest.

Appendix A

Table A1. Glossary of symbols used.

Symbol	Units	Description
μ_a	cm^{-1}	absorption coefficient
μ_s	cm^{-1}	scattering coefficient
Θ_s	rad	deviation angle during the scattering

Table A1. *Cont.*

Symbol	Units	Description
g	–	anisotropy factor $g = \langle \cos(\Theta_s) \rangle$
μ'_s	cm^{-1}	reduced scattering coefficient $\mu'_s = (1 - g)\ \mu_s$
r	cm or mm	distance from an isotropic radiation source to its registration point in an infinite scattering medium
Φ_S,	W	radiation flux generated by the light source used
$\Phi_{\lambda S}$,	W/μm	spectral density of the radiation flux generated by the light source used
$\Phi_{\lambda HL}$, $\Phi_{\lambda LED}$	W/μm	spectral density of the radiation flux at the end of the fibre generated by a halogen lamp or LED
M	W/cm^2	surface radiation luminosity
L	$W/(cm^2 \cdot sr)$	surface radiation brightness
ϕ	W/cm^2	illumination of an elementary area by a light flux from a point isotropic emitter (scattered by the medium), provided that the normal to the area coincides with the direction to the isotropic emitter
J	W/cm^2	density of radiation flux from the elementary area of the scattering medium in the direction of the unit vector
D	cm or mm	optical diffusion length, i.e., the distance at which ϕ is decreased by a factor of e due to scattering and absorption, i.e., $D \approx 1/[3(\mu'_s + \mu_a)]$
μ_{eff}	cm^{-1}	effective coefficient of the attenuation of radiation by the medium $\mu_{eff} = \sqrt{\mu_a / D} = \sqrt{3\mu_a(\mu_a + \mu'_s)}$
n_{sm}	–	real part of the complex spectral refractive index of the sample
n_{ex}	–	refractive index of the medium from which radiation is introduced into the sample of the scattering material
Θ	rad	angle of incidence of radiation from the scattering medium relative to the normal to the surface directed into the medium
Θ_c	rad	angle of total internal reflection of radiation
Θ_{uh}, ϕ_{uh}	rad	elevation and azimuth angles used when integrating the radiation emerging from the scattering medium over the solid angle Ω within the upper hemisphere
z	cm or mm	depth z in the scattering sample
λ	nm	wavelength of light radiation
$\mu^*_a(\lambda)$, $\mu'^*_s(\lambda)$	cm^{-1}	spectral coefficients of absorption and reduced scattering varied during the fitting
m^*_λ	–	variable exponent in approximation expression $\mu'^*_s(\lambda)$
λ_0	nm	wavelength of light radiation used when setting the variable spectral coefficient of reduced scattering, for example, in the form $\mu'^*_s(\lambda) = \mu'^*_s(\lambda_0) \cdot (\lambda_0/\lambda)^{m^*_\lambda}$
ρ	cm or mm	distance between the point of input of radiation into a sample of a finely dispersed medium or material and the point of recording of diffusely scattered radiation emerging from the medium
ρ_k	cm or mm	set of distances used between the fixed emitting and movable receiving probes
$k_\phi(n_{sm})$	–	coefficient that takes into account the influence of the refractive index of the scattering medium n_{sm} on the component of the local diffuse reflection coefficient $R(\rho)$, the value of which is determined by the illumination of the medium created in the registration point directly by the radiation of an isotropic point source
$k_j(n_{sm})$	–	coefficient similar to $k_\phi(n_{sm})$, which is determined by the illumination of the medium at the registration point, created due to the diffusion of photons from a more illuminated area of the scattering medium
R_{eff}	–	effective reflection coefficient of radiation entering the interface between the media from the scattering medium into the back hemisphere, i.e., back into the scattering medium
A	–	ratio $A = (1 + R_{eff})/(1 - R_{eff})$ used when setting the boundary conditions for $\phi(\rho)$
z_b	cm or mm	height of placement of the extrapolated boundary $z_b = 2A \cdot D$ above the surface of the sample of the scattering medium
$R_L(\lambda,\rho_k)$	$m^{-2} \cdot sr^{-1}$	spectral–spatial local profile of diffuse reflection per unit solid angle
$R(\lambda,\rho_k)$	mm^{-2}	spectral–spatial profile of diffuse reflection of a scattering semi-infinite medium
$R_m(\lambda_i,\rho_k)$	mm^{-2}	measured spectral–spatial profile of diffuse reflection of the material sample under study
$R\{\mu^*_a[\mu'^*_s(\lambda_i)],\rho_k\}$	mm^{-2}	spectral–spatial profile of diffuse reflection modelled during fitting
λ_{aL}	nm	left (short-wavelength) boundary of the part of the spectrum used in fitting the simulated profiles to the measured ones $R_m(\lambda_i,\rho_k)$

Table A1. *Cont.*

Symbol	Units	Description
k_M	–	factor that takes into account the effect of the state of the sample surface (glossy or rough) on the obtained values $R_m(\lambda,\rho_k)$, $k_M \leq 1$
r_{tr}	–	reflection coefficient of the input radiation directly from the sample surface (specular component)
$D_s(\lambda_i)$	–	digital readings at the output of the spectrometer corresponding to the code received by the analogue-to-digital converter of the spectrometer from the i-th photosensitive element of the spectrometer linear CCD array detector
τ_k	ms	set of used exposure times during recording $R_m(\lambda_i,\rho_k)$
$V(\lambda_i,\rho_k)$	ms^{-1}	family of recorded spectral dependencies $V(\lambda_i,\rho_k) = D_s(\lambda_i,\rho_k)/\tau_k$
λ_m	nm	wavelength corresponding to the maximum absolute spectral sensitivity $S_L(\lambda_i)$ of the spectral equipment used
$S_L(\lambda_i)$	$\frac{W \cdot ms}{cm^2 \cdot sr \cdot \mu m}$	absolute spectral sensitivity of the applied spectral equipment in terms of the spectral density of the radiation brightness $L(\lambda)$, which is determined when it is calibrated according to the reference emitter [36,37] and is used to calculate the spectral density of the brightness of the surface radiation $L(\lambda_i,\rho_k) = S_L(\lambda_i)V(\lambda_i,\rho_k)$
$f_{R,\lambda}$	–	residual function used when fitting the simulated profile $R\{\mu^*{}_a[\mu'^*{}_s(\lambda_i)],\rho_k\}$ to the measured one $R_m(\lambda_i,\rho_k)$
$\sigma_{R,\Delta\mu_a}$	–	root-mean-square deviation of residual function at wavelength λ_0 when varying the parameters $\mu'^*{}_s(\lambda)$ $\sigma_{R,\Delta\mu_a}\left[\mu'^*_s(\lambda_0), m^*_\lambda\right] = \sqrt{\sum_{\lambda_i}\left\{f_{R,\lambda}\left[\mu'^*_s(\lambda_0), m^*_\lambda, \lambda_i\right]\right\}}$

References

1. Aernouts, B.; Van Beers, R.; Watté, R.; Huybrechts, T.; Lammertyn, J.; Saeys, W. Visible and near-infrared bulk optical properties of raw milk. *J. Dairy Sci.* **2015**, *98*, 6727–6738. [CrossRef]
2. Nicolaï, B.M.; Beullens, K.; Bobelyn, E.; Peirs, A.; Saeys, W.; Theron, K.I.; Lammertyn, J. Nondestructive measurement of fruit and vegetable quality by means of NIR spectroscopy: A review. *Postharvest Biol. Technol.* **2007**, *46*, 99–118. [CrossRef]
3. Vaudelle, F.; L'Huillier, J.-P.; Askoura, M.L. Light source distribution and scattering phase function influence light transport in diffuse multi-layered media. *Opt. Commun.* **2017**, *392*, 268–281. [CrossRef]
4. Do Trong, N.N.; Erkinbaev, C.; Tsuta, M.; De Baerdemaeker, J.; Nicolaï, B.; Saeys, W. Spatially resolved diffuse reflectance in the visible and near-infrared wavelength range for non-destructive quality assessment of 'Braeburn' apples. *Postharvest Biol. Technol.* **2014**, *91*, 39–48. [CrossRef]
5. Doornbos, R.M. The determination of in vivo human tissue optical properties and absolute chromophore concentrations using spatially resolved steady-state diffuse reflectance spectroscopy. *Phys. Med. Biol.* **1999**, *44*, 967–981. [CrossRef] [PubMed]
6. Thueler, P.; Charvet, I.; Bevilacqua, F.; Ghislain, M.S.; Ory, G.; Marquet, P.; Meda, P.; Vermeulen, B.; Depeursinge, C. In vivo endoscopic tissue diagnostics based on spectroscopic absorption, scattering, and phase function properties. *J. Biomed. Opt.* **2003**, *8*, 495–503. [CrossRef] [PubMed]
7. Abookasis, D.; Zafrir, E.; Nesher, E.; Pinhasov, A.; Sternklar, S. Diffuse near-infrared reflectance spectroscopy during heatstroke in a mouse model: Pilot study. *J. Biomed. Opt.* **2012**, *17*, 105009-1–105009-11. [CrossRef]
8. Abookasis, D.; Shochat, A.; Mathews, S.M. Monitoring hemodynamic and morphologic responses to closed head injury in a mouse model using orthogonal diffuse near-infrared light reflectance spectroscopy. *J. Biomed. Opt.* **2013**, *18*, 04503-1–04503-11. [CrossRef]
9. Bevilacqua, F.; Piguet, D.; Marquet, P.; Gross, J.D.; Tromberg, B.J.; Depeursinge, C. In vivo local determination of tissue optical properties: Applications to human brain. *Appl. Opt.* **1999**, *38*, 4939–4950. [CrossRef]
10. Ishimaru, A. *Wave Propagation and Scattering in Random Media*; Wiley-IEEE Press: Piscataway, NJ, USA, 1997.
11. Tuchin, V. *Tissue Optics: Light Scattering Methods and Instruments for Medical Diagnostics*, 3rd ed.; SPIE Press: Bellingham, WA, USA, 2015.
12. Ripoll, J.; Yessayan, D.; Zacharakis, G.; Ntziachristos, V. Experimental determination of photon propagation in highly absorbing and scattering media. *J. Opt. Soc. Am. A Opt. Image Sci. Vis.* **2005**, *22*, 546–551. [CrossRef] [PubMed]
13. D'Eon, E.; Irving, G. A quantized-diffusion model for rendering translucent materials. *ACM Trans. Graph. (TOG)* **2011**, *30*, 1–14. [CrossRef]
14. Farrell, T.J.; Patterson, M.S.; Wilson, B.C. A diffusion theory model of spatially resolved, steady-state diffuse reflectance for the noninvasive determination of tissue optical properties in vivo. *Med. Phys.* **1992**, *19*, 881–888. [CrossRef] [PubMed]
15. Jacques, S. Video reflectometry to specify optical properties of tissue in vivo. In *Medical Optical Tomography: Functional Imaging and Monitoring, Proceedings of the SPIE, Bellingham, WA, USA, 15 August 1993*; SPIE Optical Engineering Press: Bellingham, WA, USA, 1993; Volume 10311, pp. 103110D-1–103110D-16. [CrossRef]

16. Haskell, R.C.; Svaasand, L.O.; Tsay, T.-T.; Feng, T.-C.; McAdams, M.S.; Tromberg, B.J. Boundary Conditions for the Diffusion Equation in Radiative Transfer. *J. Opt. Soc. Am. A* **1994**, *11*, 2727–2741. [CrossRef] [PubMed]
17. Kumar, G.; Schmitt, J.M. Optimal probe geometry for near-infrared spectroscopy of biological tissue. *Appl. Opt.* **1997**, *36*, 2286–2293. [CrossRef]
18. Farrell, T.J.; Patterson, M.S. Experimental verification of the effect of refractive index mismatch on the light fluence in a turbid medium. *J. Biomed. Opt.* **2001**, *6*, 468–473. [CrossRef]
19. Jacques, S.L. Modeling tissue optics using Monte Carlo modeling: A tutorial. In *Optical Interactions with Tissue And Cells Xix, San Jose, CA, USA, 21–23 January 2008*; SPIE Optical Engineering Press: Bellingham, WA, USA, 2008; Volume 6854, p. 68540T. [CrossRef]
20. Liang, S.; Shimizu, K. Development of a technique to measure local scattering in turbid media using backscattered light at the surface for noninvasive turbidity evaluation of blood in subcutaneous blood vessels. *Jpn. J. Appl. Phys.* **2021**, *60*, 022002. [CrossRef]
21. Cappon, D.J.; Farrell, T.J.; Fang, Q.; Hayward, J.E. Fiber-optic probe design and optical property recovery algorithm for optical biopsy of brain tissue. *J. Biomed. Opt.* **2013**, *18*, 107004-1–107004-10. [CrossRef]
22. Kanick, S.C.; Sterenborg, H.J.C.M.; Amelink, A. Empirical model of the photon path length for a single fiber reflectance spectroscopy device. *Opt. Express* **2009**, *17*, 860–871. [CrossRef]
23. Piao, D.; Patel, S. Simple empirical master–slave dual-source configuration within the diffusion approximation enhances modeling of spatially resolved diffuse reflectance at short-path and with low scattering from a semi-infinite homogeneous medium. *Appl. Opt.* **2017**, *56*, 1447–1452. [CrossRef]
24. Seo, I.; Hayakawa, C.; Venugopalan, V. Radiative transport in the delta-P1 approximation for semi-infinite turbid media. *Med. Phys.* **2008**, *35*, 681–693. [CrossRef]
25. Amelink, A.; Haringsma, J.; Sterenborg, H. Noninvasive measurement of oxygen saturation of the microvascular blood in Barrett's dysplasia by use of optical spectroscopy. *Gastroint. Endosc.* **2009**, *70*, 1–6. [CrossRef] [PubMed]
26. Kanick, S.C.; van der Leest, C.; Djamin, R.S.; Janssens, A.M.; Hoogsteden, H.C.; Henricus, J.C.M.; Sterenborg, A.; Amelink, J.; Aerts, G.J.V. Characterization of Mediastinal Lymph Node Physiology In Vivo by Optical Spectroscopy during Endoscopic Ultrasound-Guided Fine Needle Aspiration. *J. Thorac. Oncol.* **2010**, *5*, 981–987. [CrossRef]
27. Lisenko, S.A.; Firago, V.A.; Kugeiko, M.M.; Kubarko, A.I. Determination of structural and morphological parameters of human bulbar conjunctiva from optical diffuse reflectance spectra. *J. Appl. Spectrosc.* **2016**, *83*, 617–626. [CrossRef]
28. Lisenko, S. Methods for Optical Diagnostics of Biological Objects, BSU, Minsk. 2014. Available online: http://elib.bsu.by/handle/123456789/114155 (accessed on 20 April 2023). (In Russian)
29. Mishchenko, M.I. *Radiative Transfer: A New Look of the Old Theory*; Radiative Transfer, V., Menguç, M.P., Selcuk, N., Eds.; Begell House: New York, NY, USA; Danbury, CT, USA, 2007; pp. 1–30.
30. Mishchenko, M.I. "Independent" and "dependent" scattering by particles in a multi-particle group. *OSA Contin.* **2018**, *1*, 243–260. [CrossRef]
31. Shendeleva, M. Influence of boundary conditions on photon diffusion through an interface between two turbid media with different refractive indices. *J. Opt. Soc. Am.* **2010**, *7*, 1521–1528. [CrossRef] [PubMed]
32. Aronson, R.; Corngold, N. Photon diffusion coefficient in an absorbing Medium. *J. Opt. Soc. Am.* **1999**, *16*, 1066–1071. [CrossRef] [PubMed]
33. Groenhuis, R.; Ferwerda, H.; Bosch, J. Scattering and absorption of turbid materials determined from reflection measurements. 1: Theory. *Appl. Opt.* **1983**, *22*, 2456–2462. [CrossRef] [PubMed]
34. Firago, V.A.; Shuliko, K.I. Application of the Diffusion Approximation in Research of Optical Properties of Condensed Finely Dispersed Environment. In Proceedings of the XIII International Scientific Conference "Quantum Electronics", Minsk, Belarus, 22–26 November 2021; pp. 329–332. Available online: https://elib.bsu.by/handle/123456789/271782 (accessed on 20 April 2023).
35. Weidner, V.; Hsia, J. Reflection properties of pressed polytetrafluoroethylene powder. *J. Opt. Soc. Am.* **1981**, *71*, 856–861. [CrossRef]
36. Firago, V.; Hotra, O.; Sakovich, I. Radiometric calibration of fiber optic spectrophotometers. In Proceedings of the Optical Fibers and Their Applications 2018, Naleczow, Poland, 20–23 November 2018; SPIE Optical Engineering Press: Bellingham, WA, USA, 2019; p. 1104516. [CrossRef]
37. Firago, V.A.; Levkovich, N.V.; Shuliko, K.I. Diffuse Reflectance Spectrophotometers Based on C12880MA and C11708MA Mini-Spectrometers Hamamatsu. *Devices Methods Meas.* **2022**, *13*, 50–59. [CrossRef]
38. Jacques, S.L. Simple theory and rules of thumb for dosimetry during therapy. In Proceedings of the Photodynamic Therapy: Mechanisms, Los Angeles, CA, USA, 5–20 January 1989; SPIE Optical Engineering Press: Bellingham, WA, USA, 1989; Volume 1065, pp. 100–108. [CrossRef]
39. Sultanova, N.G.; Kasarova, S.N.; Nikolov, I.D. Characterization of optical properties of optical polymers. *Opt. Quant. Electron.* **2013**, *45*, 212–232. [CrossRef]

40. Firago, V.A.; Wojcik, W.; Dzhunisbekov, M.S. Monitoring of the Metal Surface Temperature during Laser Processing. *Russ. Metall.* **2019**, *11*, 1224–1230. [CrossRef]
41. Hotra, O.; Firago, V.; Levkovich, N.; Shuliko, K. Investigation of the Possibility of Using Microspectrometers Based on CMOS Photodiode Arrays in Small-Sized Devices for Optical Diagnostics. *Sensors* **2022**, *22*, 4195. [CrossRef] [PubMed]